

Ultra Reliable UAV Communication Using Altitude and Cooperation Diversity

Mohammad Mahdi Azari, Fernando Rosas, Kwang-Cheng Chen, and Sofie Pollin

Abstract—The use of unmanned aerial vehicles (UAVs) serving as aerial base stations is expected to become predominant in the next decade. However, in order, for this technology, to unfold its full potential, it is necessary to develop a fundamental understanding of the distinctive features of air-to-ground (A2G) links. As a contribution in this direction, this paper proposes a generic framework for the analysis and optimization of the A2G systems. In contrast to the existing literature, this framework incorporates both height-dependent path loss exponent and small-scale fading, and unifies a widely used ground-to-ground channel model with that of A2G for the analysis of large-scale wireless networks. We derive analytical expressions for the optimal UAV height that minimizes the outage probability of an arbitrary A2G link. Moreover, our framework allows us to derive a height-dependent closed-form expression for the outage probability of an A2G cooperative communication network. Our results suggest that the optimal location of the UAVs with respect to the ground nodes does not change by the inclusion of ground relays. This enables interesting insights about the deployment of future A2G networks, as the system reliability could be adjusted dynamically by adding relaying nodes without requiring changes in the position of the corresponding UAVs. Finally, to optimize the network for multiple destinations, we derive an optimum altitude of the UAV for maximum coverage region by guaranteeing a minimum outage performance over the region.

Index Terms—Air-to-ground (A2G) communication, unmanned aerial vehicle (UAV), aerial base station, outage probability, Rician fading, inverse Marcum Q-function, cooperative communication, Poisson point process (PPP).

I. INTRODUCTION

AERIAL telecommunication platforms are being increasingly used as an innovative method to enable robust and reliable communication networks. Facebook [1] and Google [2] have been planning to establish massive networks of unmanned aerial vehicles (UAVs) to provide broadband connectivity to remote areas. Amazon has announced a research plan to explore new means of delivery service making use of small UAVs to shorten the delivery time [3]. The ABSOLUTE project in Europe aims to provide a low latency and large coverage networks using aerial base stations for capacity enhancements and public safety during temporary events [4].

Manuscript received December 21, 2016; revised May 14, 2017 and July 19, 2017; accepted August 17, 2017. Date of publication August 29, 2017; date of current version January 13, 2018. The associate editor coordinating the review of this paper and approving it for publication was A. Nallanathan. (Corresponding author: Mohammad Mahdi Azari.)

M. M. Azari and S. Pollin are with KU Leuven, Leuven 3001, Belgium (e-mail: mahdi.azari@kuleuven.be).

F. Rosas is with Imperial College London, London SW7 2AZ, U.K.

K.-C. Chen is with the University of South Florida, Tampa, FL 33620 USA.

Color versions of one or more of the figures in this paper are available online at <http://ieeexplore.ieee.org>.

Digital Object Identifier 10.1109/TCOMM.2017.2746105

UAVs have also been used in the context of Internet of Things (IoT) to assist low power transmitters to send their data to a destination [5], [6], and to enable energy-efficient communication [7], [8]. Moreover, it has been shown that UAVs as low altitude platforms (LAPs) can be integrated into a cellular network to compensate cell overload or site outage [9], to enhance public safety in the failure of the base stations [10], and to boost the capacity of the network. The coverage performance of drone deployment in cellular networks is thoroughly studied in [11]. Finally, an overview of UAV-assisted wireless communication and networking can be found in [12].

A. Related Work and Motivation

To enable the deployment of UAVs network, it is important to model the reliability and coverage of the aerial platforms. In particular, recent studies have shown that the location and height of a UAV can significantly affect the air-to-ground (A2G) link reliability. In [13] the optimal placement of UAVs, acting as relays, is studied without considering the impact of altitude on its coverage range. In [14] the trajectory of a mobile UAV relaying is optimized for maximum throughput. In [15] the impact of altitude on the coverage range of UAVs is studied, without providing a closed-form expression showing the dependency of the coverage radius to the system parameters. An optimum placement of multiple UAVs for maximum number of covered users is investigated in [16], [17], where in [17] the coverage lifetime is also taken into account. All these works [15]–[17], however, ignore the stochastic effects of multipath fading, which is an essential feature of an A2G communication link [18]. Moreover, the path loss modeling is based on free space conditions, making it impossible to address the performance for low altitude scenarios which is of practical importance due to the regulation constraints.

Besides the link characterization, the next step to further improve the reliability of a UAV link is to study the cooperation of the UAV with the existing terrestrial network. Cooperative communication techniques are known to significantly enhance the reliability of a wireless system. Three main cooperation protocols named amplify-and-forward (AF), decode-and-forward (DF) and coded cooperation (CC) together with outage performance have been studied in [19]–[24], relying on identical propagation and fading models for the first and second hops of the cooperative communication link. In [24] the results show that CC and DF outperform AF in terms of outage performance, however more complexity is imposed to the system. In fact, DF has a moderate complexity and

outage performance among these strategies and discards the disadvantage of AF where the noise is amplified in relays. All of these studies focus on terrestrial cooperative networks, however in this paper we incorporate ground-to-ground (G2G) and A2G communication links in an A2G *cooperative communication* system. To the best of our knowledge, this is the first paper investigating the outage performance of such network as function of UAV altitude. This allows to quantify the benefits of ground relaying nodes at every altitude in A2G networks and enables to measure the performance gains when aerial and ground nodes cooperate. However, a fair and accurate analysis of an A2G cooperative network would require a generic framework which is valid for both G2G and A2G communication links, enabling to consider a continuum of different propagation conditions.

B. Contributions

In this paper, we consider a UAV as an aerial base station that aims to serve ground nodes in downlink. We propose a generic framework that extends a widely used model for G2G wireless links towards A2G channels. Moreover, this framework considers an altitude-dependent path loss exponent and fading function, supplementing the existent A2G channel models. Using this analytical framework, we also significantly extend and refine our previous works [25]–[27]. In fact, the results presented in our initial study [25] are restricted to consider the same path loss exponent at different altitudes, which is an unrealistic assumption considering the different propagation environments. Moreover, we derive the height of the UAV for minimum outage probability at every user location and the optimum UAV altitude resulting in maximum coverage radius, which are not presented in [26].

We also extend our previous work by analyzing an A2G cooperative network where each communication link possesses different channel statistics. To this end, we analyze the height-dependent outage performance of the network when adopting a DF protocol at the ground relays, deriving a lower bound for the end-to-end outage probability. We quantify the benefits of the cooperative relaying, showing that the reliability of A2G communication strongly benefits from the introduction of ground relays. Furthermore, we show that the optimal transmission height is not much affected by the existence of ground relays, which allows to include them dynamically without losing the optimality of the UAV location. Finally, we study the optimum height-dependent power allocation for relaying and cooperative communication in order to maximize the coverage region.

We note that in our model we could also consider aerial relays. However, as is reported in [11] and [28], the UAVs can be heavily affected by ground interferers due to the high probability of LoS. This, in turn, limits the achievable performance of aerial receivers. Moreover, in many scenarios ground relays can be widely available as part of an existing terrestrial networks, contrasting with the case for the aerial relaying nodes which have to be added by the network controller. Therefore, leveraging ground relays appears to be more practical in the field deployment, while this proposed

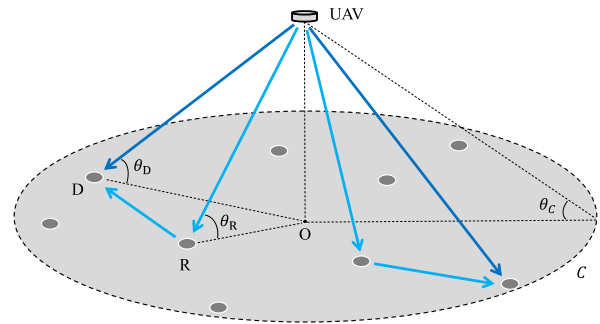


Fig. 1. A typical air-to-ground (A2G) wireless networking using a UAV in the presence of randomly distributed ground relays over the coverage region C . In our analysis, we consider both a ground destination (D), as well as cooperative relays (R).

framework is general to allow us to extend the results for aerial relay to the ground as well.

The rest of this paper is organized as follows. In Section II we present the system model. The problem is stated in Section III. The system outage performance and the optimum altitude in direct A2G communication links are derived in Section IV followed by Section V where the outage performance of the relaying strategy and the corresponding lower bound are analyzed. Our results are discussed and confirmed in Section VI. Finally, the main conclusions are presented in Section VII.

II. SYSTEM MODEL

We consider a cellular system where a UAV provides wireless access to terrestrial mobile devices, serving as an aerial base station. The UAV is placed in an adjustable altitude h , aiming to communicate with a ground node D either directly or through a terrestrial relay R, as illustrated in Figure 1. The elevation angles of the UAV with regard to D and R are denoted as θ_D and θ_R , respectively. The relaying nodes are randomly distributed, following a Poisson point process (PPP)¹ of a fixed density λ . For communication, however, we focus on a disk C centered at the projection of the UAV on the ground, denoted as O. This region represents a UAV cell or the coverage area of the UAV and hence only the nodes within C are considered as potential relays to assist the UAV. A polar coordinate system with the origin at O is considered, so that the location of the nodes D and R can be described by (r_D, φ_D) and (r_R, φ_R) respectively. Please note that in our system model we assume the availability of cell planning to ensure that cells of multiple UAVs, and aerial and terrestrial cells do not overlap.

In the sequel, Section II-A describes the channel model and the corresponding characteristics of fading and path loss in terms of altitude are discussed in Section II-B.

A. Channel Modeling

The wireless channel between any pair of nodes is assumed to experience small-scale fading and large-scale path loss.

¹A Poisson field of nodes means that the nodes are randomly, uniformly, and independently distributed over the spatial domain such that the number of nodes within any bounded area in the space is a Poisson random variable.

Therefore, the instantaneous signal-to-noise ratio (SNR) between the UAV, denoted as U, and a ground receiver X, which is either R or D, can be modeled as

$$\Gamma_{UX} = \frac{AP_U}{N_0 \ell_{UX}^{\alpha_{UX}}} \Omega_{UX}; \quad X \in \{D, R\}, \quad (1)$$

where P_U is the UAV's transmit power, N_0 is the noise power, ℓ_{UX} is the distance between the UAV and the node X, α_{UX} is the path loss exponent, A is a constant which depends on the system parameters such as operating frequency and antenna gain, and Ω_{UX} is the fading power where $\bar{\Omega}_{UX} = 1$.

In order to model the small-scale fading between the UAV and any ground node X, a Rician distribution is an adequate choice due to the possible combination of LoS and multipath scatterers that can be experienced at the receiver [18], [29], [30]. Using this model, Ω_{UX} adopts a non-central chi-square probability distribution function (PDF) expressed as [31]

$$f_{\Omega_{UX}}(\omega) = \frac{(K_{UX} + 1)e^{-K_{UX}}}{\bar{\Omega}_{UX}} \exp\left(-\frac{(K_{UX} + 1)\omega}{\bar{\Omega}_{UX}}\right) \times I_0\left(2\sqrt{\frac{K_{UX}(K_{UX} + 1)\omega}{\bar{\Omega}_{UX}}}\right); \quad \omega \geq 0. \quad (2)$$

Above $I_0(\cdot)$ is the zero-order modified Bessel function of the first kind, and K_{UX} is the Rician factor defined as the ratio of the power in the LoS component to the power in the non-LoS multipath scatterers. In this representation, K_{UX} reflects the severity of the fading. In effect, if $K_{UX} = 0$, the equation (2) is reduced to an exponential distribution indicating a Rayleigh fading channel, while if $K_{UX} \rightarrow \infty$ the channel converges to an additive white Gaussian noise (AWGN) channel. Accordingly, more severe fading conditions correspond to a channel with lower K_{UX} .

Following a similar rationale, the instantaneous SNR between an arbitrary relaying node R as the transmitter and the receiver D can be modeled as

$$\Gamma_{RD} = \frac{AP_R}{N_0 \ell_{RD}^{\alpha_{RD}}} \Omega_{RD}, \quad (3)$$

where P_R is the relay's transmit power which is assumed to be the same for all the relaying nodes, ℓ_{RD} is the distance between R and D, α_{RD} is the G2G path loss exponent between R and D, and Ω_{RD} is the fading power modeled by a Rician distribution with $\bar{\Omega}_{RD} = 1$, where its PDF can be written using (2) but considering a different Rician factor denoted as K_{RD} . Finally, it is assumed that the fading statistics between different pair of nodes are independent.

B. Rician Factor and Path Loss Exponent Modeling

Intuitively, the height of the UAV affects the propagation characteristics of the A2G communication link since the LoS condition and the environment between U and X alter as θ_X varies. It has been shown that the elevation angle of the UAV with respect to the ground node plays a dominant role in determining the Ricean factor [32], [33]. Consequently, we model the Ricean factor as a function of the elevation angle by introducing the non-decreasing function $K_{UX} = K(\theta_X)$. Indeed, a larger θ_X implies a higher LoS contribution and less

multipath scatterers at the receiver resulting in a larger K_{UX} . Thus, G2G communication ($\theta_X = 0$) experience the most severe multipath conditions and hence K_{UX} takes its minimal value $\kappa_0 = K(0)$, whereas at $\theta_X = \pi/2$ it adopts the maximum value $\kappa_{\pi/2} = K(\pi/2)$. Note that $K_{RD} = \kappa_0$, as it corresponds to a G2G link.

Following a similar rationale, the path loss is also influenced by the elevation angle such that α_{UX} might decrease as the UAV's elevation angle θ_X increases. In this way, G2G links, where $\theta_X = 0$, endure the largest α_{UX} while at $\theta_X = \pi/2$ the value of α_{UX} is the smallest. Therefore, we model the path loss exponent dependency on the elevation angle by introducing a non-increasing function of $\alpha_{UX} = \alpha(\theta_X)$ and define the shorthand notations $\alpha_0 = \alpha(0)$ and $\alpha_{\pi/2} = \alpha(\pi/2)$. Accordingly, G2G links have $\alpha_{rd} = \alpha_0$.

The analysis presented in the following sections is based on a general dependency of $K(\theta_X)$ and $\alpha(\theta_X)$ on θ_X , in order to provide comprehensive results which are valid over a variety of conceivable scenarios. Therefore, in any concrete scenario the results can be instantiated by determining the estimated functional form for $K(\theta_X)$ and $\alpha(\theta_X)$. However, in Section VI we adopt a particular parameterized family of functions in order to illustrate our results.

III. PROBLEM STATEMENT

An A2G channel benefits from a lower path loss exponent and lighter small-scale fading compared to a G2G link, while having a longer link length which deteriorates the received SNR. Interestingly, these two opposite effects can be balanced by optimizing the UAV height. Thus, our fundamental concern is to find the best position of a UAV for optimizing the link reliability, and to study if such an optimized positioning can have a positive impact on the UAV coverage area. Finally, we are also interested in studying the effect of ground relays –as a means of reliability enhancement and coverage extension– on the optimal UAV altitude.

Link reliability is usually evaluated using the outage probability, which is defined as

$$\mathcal{P}_{\text{out}}^Y \triangleq \mathbb{P}(\Gamma \leq \zeta), \quad (4)$$

where $\mathbb{P}(E)$ indicates the probability of an event E, Γ is the instantaneous SNR at the receiver, ζ is the SNR threshold which depends on the sensitivity of the receiver, and $Y \in \{\text{dc}, \text{rc}, \text{cc}\}$ indicates the strategy employed for communication which is an abbreviation for direct communication, relaying communication and cooperative communication, respectively.

A. Optimal Altitude for an Arbitrary Destination

The A2G channel characteristic and hence the received SNR at an arbitrary ground destination D is dependent on the relative position of the UAV to D determined by h and r_D , and hence the outage probability can be written as $\mathcal{P}_{\text{out}}^Y = \mathcal{P}_{\text{out}}^Y(r_D, h)$. At a given and arbitrary r_D , the optimum altitude of the UAV \tilde{h}_D^Y for maximum reliable link is defined as

$$\tilde{h}_D^Y = \arg \min_{h \in [0, \infty)} \mathcal{P}_{\text{out}}^Y(r_D, h); \quad Y \in \{\text{dc}, \text{rc}, \text{cc}\}. \quad (5)$$

This optimal altitude² depends on the distance r_D and might vary for destinations at different locations.

B. Optimum Altitude for Multiple Destinations

Since the optimal altitude varies for different destination locations, considering a scenario with multiple destinations to be served simultaneously, we define an optimum altitude at which a minimum QoS is guaranteed for all the destinations. To this end, an optimum altitude is determined to maximize the coverage region and hence to increase the number of ground users to be covered in real-time. Accordingly, for a given altitude h the radius of UAV's coverage area \mathcal{C} is defined as the maximum distance r_D within which the outage probability remains below or equals to a target ε . For a larger r_D the outage probability $\mathcal{P}_{\text{out}}^Y(r_D, h)$ is higher due to the larger path loss and more severe fading. Thus, the boundary of the coverage region is characterized by (r_D, φ_D) s that $\varphi_D \in [0, 2\pi]$ and r_D meets

$$\mathcal{P}_{\text{out}}^Y(r_D, h) = \varepsilon. \quad (6)$$

For a given h , we denote the radius r_D satisfying the above equation as r_C^Y . The set of all pairs (r_C^Y, h) that meet the above equation constitute a system *configuration space* denoted as \mathcal{S}^Y . We intend to obtain the maximum coverage radius \tilde{r}_C^Y in \mathcal{S}^Y , by locating the UAV at the optimum altitude \tilde{h}_C^Y . To this end, the problem can be formulated as

$$\begin{aligned} \tilde{r}_C^Y &= \max_{h \in [0, \infty)} r_C^Y, \\ \text{s.t. } &(r_C^Y, h) \in \mathcal{S}^Y \end{aligned} \quad (7)$$

and \tilde{h}_C^Y is the altitude that $(\tilde{r}_C^Y, \tilde{h}_C^Y) \in \mathcal{S}^Y$, i.e. the optimal altitude at which the coverage radius is maximized.

Please note that \tilde{r}_C^Y is the maximum coverage radius for being able to serve the maximum number of destinations at the same time. In a different approach, a UAV can use its movement capability to a larger total area served by different locations where the UAV is hovering to temporary serve the ground users. However, in this case some destinations might not be able to connect to the UAV instantly and some delay will be imposed to the network since the speed of UAV is limited. The result of this paper can then be used for a delay-tolerant network design, focusing on a trade-off between sum coverage area and delay. In this paper, we only focus on the scenario where delay is not tolerated and a UAV is hovering at a constant location.

IV. DIRECT AIR-TO-GROUND COMMUNICATION

This section we analyze the outage probability of transmissions going directly from the UAV to the destination. The outage probability is studied as function of UAV altitude in Section IV-A and then the results are used to investigate the optimal placement of the UAV for maximum reliability and range of communication in Section IV-B.

²The altitude of a UAV can be assessed by using a GPS module attached to the UAV or by using air-pressure sensor that can be of help to measure the altitude.

A. Height-Dependent Outage Probability

Following (4) the direct communication outage probability of the UAV-D link $\mathcal{P}_{\text{out}}^{\text{dc}}$ is defined as $\mathcal{P}_{\text{out}}^{\text{dc}} = \mathbb{P}(\Gamma_{\text{UD}} \leq \xi)$. By using (1) and (2), the outage probability can be rewritten as

$$\begin{aligned} \mathcal{P}_{\text{out}}^{\text{dc}}(r_D, h) &= \mathbb{P}\left(\frac{AP_U}{N_0 \ell_{\text{UD}}^{\alpha_{\text{UD}}}} \Omega_{\text{UD}} \leq \xi\right) \\ &= 1 - Q\left(\sqrt{2K(\theta_D)}, \sqrt{2\xi [1 + K(\theta_D)] \ell_{\text{UD}}^{\alpha(\theta_D)} / \gamma_U}\right), \end{aligned} \quad (8)$$

where $\ell_{\text{UD}} = \sqrt{r_D^2 + h^2}$, $\theta_D = \tan^{-1}(h/r_D)$, $Q(\cdot, \cdot)$ is the first order Marcum Q-function, and γ_U is a shorthand notation for

$$\gamma_U \triangleq \frac{AP_U}{N_0}. \quad (9)$$

We propose the following theorem to solve the optimization in (5), where the position of the UAV for minimum outage probability at every r_D is obtained.

Theorem 1: For a given r_D the optimal UAV altitude \tilde{h}_D^{dc} , as defined in (5), is given by

$$\tilde{h}_D^{\text{dc}} = r_D \cdot \tan(\tilde{\theta}_D^{\text{dc}}), \quad (10)$$

where $\tilde{\theta}_D^{\text{dc}}$ is approximately obtained from

$$\begin{aligned} \sqrt{\frac{\xi}{\gamma_U} \left[\frac{r_D}{\cos(\theta_D)} \right]^{\alpha(\theta_D)}} \left[\frac{K'(\theta_D)}{K(\theta_D)} + \alpha'(\theta_D) \ln \left(\frac{r_D}{\cos(\theta_D)} \right) \right. \\ \left. + \alpha(\theta_D) \tan(\theta_D) \right] = \frac{K'(\theta_D)}{K(\theta_D)}. \end{aligned} \quad (11)$$

Proof: The proof is given in Appendix A. ■

Note that (11) shows that $\tilde{\theta}_D^{\text{dc}}$ is dependent on r_D and hence the optimal altitude $\tilde{h}_D^{\text{dc}} = r_D \cdot \tan(\tilde{\theta}_D^{\text{dc}})$ is not generally a linear function of r_D . In fact, at short distances of r_D an increase in the elevation angle θ_D could be more beneficial than that of large distances since the increase in the link length is smaller while the impact on the path loss exponent and the Rician factor is the same for any r_D . Therefore (11) leads to a larger value of $\tilde{\theta}_D^{\text{dc}}$ for a smaller r_D .

In the next subsection we obtain the maximum coverage radius of the UAV \tilde{r}_C^{dc} and the corresponding optimum altitude \tilde{h}_C^{dc} .

B. Maximum Coverage Area

The implicit relationship between h and r_C^{dc} in (6) can be rewritten using (8) as

$$Q\left(\sqrt{2K(\theta_C)}, \sqrt{2\xi [1 + K(\theta_C)] \ell_C^{\alpha(\theta_C)} / \gamma_U}\right) = 1 - \varepsilon, \quad (12)$$

where $\ell_C = \sqrt{(r_C^{\text{dc}})^2 + h^2}$, $\theta_C = \tan^{-1}(h/r_C^{\text{dc}})$. In order to find \tilde{r}_C^{dc} and \tilde{h}_C^{dc} from (7), first we determine the configuration space using the following theorem.

Theorem 2: The configuration space \mathcal{S}^{dc} is a one-dimensional curve in the r_D - h plane, which is formed by all (r_C^{dc}, h) obtained from

$$h = \Lambda(\theta_C) \cdot \sin(\theta_C), \quad (13a)$$

$$r_C^{dc} = \Lambda(\theta_C) \cdot \cos(\theta_C), \quad (13b)$$

where

$$\Lambda(\theta_C) = \left[\frac{\gamma_U y_C^2}{\xi(2+x_C^2)} \right]^{\frac{1}{\alpha(\theta_C)}}, \quad (13c)$$

$$x_C = \sqrt{2K(\theta_C)}, \quad y_C = Q^{-1}(x_C, 1-\varepsilon), \quad \theta_C \in [0, \frac{\pi}{2}]. \quad (13d)$$

Above, $Q^{-1}(x_C, \cdot)$ indicates the inverse Marcum Q -function with respect to its second argument.

Proof: Using the following auxiliary variables

$$x_C = \sqrt{2K(\theta_C)}, \quad y_C = \sqrt{2\xi [1 + K(\theta_C)] \ell_C^{\alpha(\theta_C)} / \gamma_U}, \quad (14)$$

the equation in (12) can be rewritten as $Q(x_C, y_C) = 1 - \varepsilon$ or equivalently

$$y_C = Q^{-1}(x_C, 1 - \varepsilon). \quad (15)$$

From (14) and (15) one can write

$$\ell_C = \left[\frac{\gamma_U [Q^{-1}(x_C, 1 - \varepsilon)]^2}{\xi(2+x_C^2)} \right]^{\frac{1}{\alpha(\theta_C)}} \triangleq \Lambda(\theta_C). \quad (16)$$

By using (16) in $h = \ell_C \cdot \sin(\theta_C)$ and $r_C^{dc} = \ell_C \cdot \cos(\theta_C)$ the desired result is attained. ■

Note that all elements of \mathcal{S}^{dc} can be described by exploring different values of θ_C . In fact, when $\theta_C = 0$, one obtains $h = 0$ and $r_C^{dc} = \Lambda(0)$, while h grows with θ_C reaching its maximum $h = \Lambda(\pi/2)$ when $\theta_C = \pi/2$ and $r_C^{dc} = 0$. The shape of the configuration space in r_D - h plane is illustrated in Figure 2, where $\Lambda(\theta_C)$ and θ_C are the radius and angle of \mathcal{S}^{dc} in polar coordinates respectively. This figure shows that at an elevation angle denoted as $\tilde{\theta}_C^{dc}$ the coverage radius reaches its maximum \tilde{r}_C^{dc} . In order to find $\tilde{\theta}_C^{dc}$ we simplify $\Lambda(\theta_C)$ in (13c) by proposing an approximate analytical solution for the inverse Marcum Q -function in the following lemma.

Lemma 1: The inverse Marcum Q -function with respect to its second argument, i.e. $y = Q^{-1}(x, 1 - \varepsilon)$, is approximately given by

$$y = \begin{cases} \sqrt{-2 \ln(1 - \varepsilon)} e^{\frac{x^2}{4}}; & x \leq x_0 \\ x + \frac{1}{2Q^{-1}(\varepsilon)} \ln \left[\frac{x}{x - Q^{-1}(\varepsilon)} \right] - Q^{-1}(\varepsilon); & x > x_0 \wedge Q^{-1}(\varepsilon) \neq 0 \\ x + \frac{1}{2x}; & x > x_0 \wedge Q^{-1}(\varepsilon) = 0 \end{cases} \quad (17)$$

where x_0 is the intersection of the sub-functions at $x > \max[0, Q^{-1}(\varepsilon)]$ and $Q^{-1}(\cdot)$ is the inverse Q -function.

Proof: The proof is given in Appendix B. ■

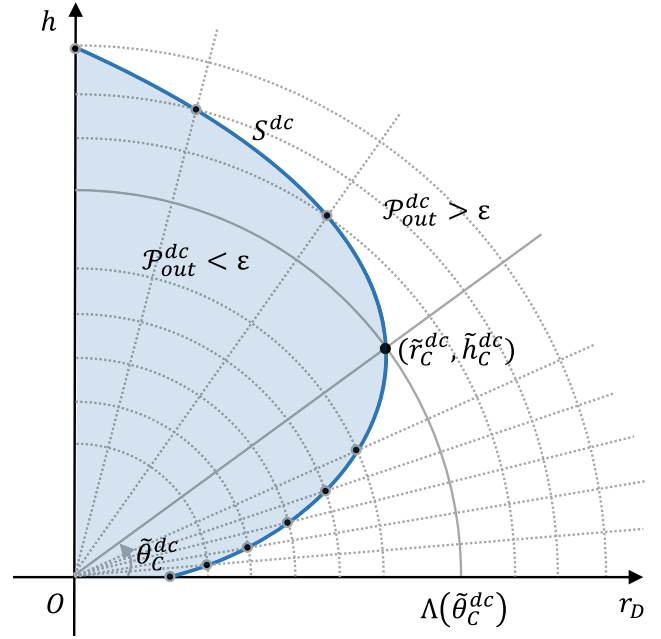


Fig. 2. Configuration space \mathcal{S}^{dc} on r_D - h plane.

Corollary 1: For $x \gg 1$, $y = Q^{-1}(x, 1 - \varepsilon)$ is approximately obtained as

$$y \cong x - Q^{-1}(\varepsilon). \quad (18)$$

Proof: For $x \gg 1$, which results in $x > x_0$, one sees that $x \gg \frac{1}{2Q^{-1}(\varepsilon)} \ln \left[\frac{x}{x - Q^{-1}(\varepsilon)} \right]$ and $x \gg \frac{1}{2x}$, and hence the desired result is obtained. ■

Now using Corollary 1 the optimum elevation angle $\tilde{\theta}_C^{dc}$ that yields the optimum altitude \tilde{h}_C^{dc} and the maximum coverage radius \tilde{r}_C^{dc} in (13) is obtained through the following theorem.

Theorem 3: The approximate optimum elevation angle of the UAV $\tilde{\theta}_C^{dc}$ at which the UAV has the maximum coverage radius \tilde{r}_C^{dc} can be found in the following implicit equation

$$\alpha(\theta_C) \tan(\theta_C) + \alpha'(\theta_C) \ln[\Lambda(\theta_C)] = 2x_C' \left(\frac{Q^{-1}(\varepsilon)}{x_C[x_C - Q^{-1}(\varepsilon)]} \right), \quad (19)$$

where $\Lambda(\theta_C)$ and x_C are defined in (13) and $\alpha'(\theta_C)$ and x_C' indicate the derivative functions with respect to θ_C .

Proof: The proof can be found in Appendix C. ■

Notice that, by using the optimum elevation angle obtained from (19) into the system equations in (13a) and (13b), the optimum altitude of the UAV \tilde{h}_C^{dc} and its maximum coverage radius \tilde{r}_C^{dc} can be obtained as

$$\tilde{h}_C^{dc} = \Lambda(\tilde{\theta}_C^{dc}) \cdot \sin(\tilde{\theta}_C^{dc}), \quad \tilde{r}_C^{dc} = \Lambda(\tilde{\theta}_C^{dc}) \cdot \cos(\tilde{\theta}_C^{dc}). \quad (20)$$

Moreover, (19) shows that $\tilde{\theta}_C^{dc}$ is independent of the transmit power P_U and the SNR threshold ξ provided that $\alpha'(\tilde{\theta}_C) \cong 0$ (c.f. Section VI). In other words, $\tilde{\theta}_C^{dc}$ and $\tilde{h}_C^{dc}/\tilde{r}_C^{dc} = \tan(\tilde{\theta}_C^{dc})$ are only determined by ε and the propagation parameters $K(\cdot)$ and $\alpha(\cdot)$ that are characterized by the type of environment and

the system parameters such as carrier frequency. Therefore, using (13) one finds that

$$\tilde{h}_C^{\text{dc}} \propto \left(\frac{P_U}{\xi} \right)^{\frac{1}{\alpha(\tilde{\theta}_C^{\text{dc}})}}, \quad \tilde{r}_C^{\text{dc}} \propto \left(\frac{P_U}{\xi} \right)^{\frac{1}{\alpha(\tilde{\theta}_C^{\text{dc}})}}. \quad (21)$$

V. AIR-TO-GROUND COMMUNICATION USING GROUND RELAYING

In this section a cooperative strategy with ground relaying is presented. The outage probability of the system is studied and an analytical lower bound is derived.

A. Ground Decode-and-Forward Relaying

We adopt the decode-and-forward (DF) opportunistic relaying method, where the data is transmitted to the destination D in two phases. In the first phase, the UAV broadcasts its data and provided that the SNR of the link between the UAV and an arbitrary relay node R_j is high enough, the relay is able to successfully decode the received signal. These relay nodes form a set called \mathcal{A} which may differ in each transmission attempt since the wireless channel between the UAV and ground nodes vary. In the second phase the best relay node R_J in \mathcal{A} which has the highest instantaneous SNR to the destination D is chosen to retransmit the received data to the destination. Therefore, we can write

$$\mathcal{A} = \{R_j \mid \Gamma_{UR_j} > \xi\}, \quad J \triangleq \arg \max_{R_j \in \mathcal{A}} \Gamma_{R_j D}, \quad (22)$$

where Γ_{UR_j} and $\Gamma_{R_j D}$ are obtained from (1) and (3) respectively. The outage probability of the relaying communication (rc) can be defined as

$$\mathcal{P}_{\text{out}}^{\text{rc}} = \mathbb{P}(\Gamma_{R_j D} \leq \xi), \quad (23)$$

which is obtained in the following theorem.

Theorem 4: The outage probability of the relaying communication $\mathcal{P}_{\text{out}}^{\text{rc}}$ can be written as

$$\mathcal{P}_{\text{out}}^{\text{rc}}(r_D, h) = e^{-\lambda[\psi_1(h) - \psi_2(r_D, h)]} \quad (24a)$$

where

$$\begin{aligned} \psi_1(h) &= 2\pi \int_0^{r_C^{\text{rc}}} r_R Q\left(\sqrt{2K(\theta_R)}, \sqrt{2[K(\theta_R) + 1]\xi\ell_{UR}^{\alpha(\theta_R)}/\gamma_U}\right) dr_R, \\ & \quad (24b) \end{aligned}$$

$$\begin{aligned} \psi_2(r_D, h) &= \int_0^{2\pi} \int_0^{r_C^{\text{rc}}} r_R \left[1 - Q\left(\sqrt{2\kappa_0}, \sqrt{2(\kappa_0 + 1)\xi\ell_{RD}^{\alpha_0}/\gamma_R}\right) \right] \\ & \quad \times Q\left(\sqrt{2K(\theta_R)}, \sqrt{2[K(\theta_R) + 1]\xi\ell_{UR}^{\alpha(\theta_R)}/\gamma_U}\right) dr_R d\varphi_R, \\ & \quad (24c) \end{aligned}$$

$$\ell_{UR} = \sqrt{r_R^2 + h^2}, \quad \ell_{RD} = \sqrt{r_R^2 + r_D^2 - 2r_R r_D \cos(\varphi_R - \varphi_D)}, \quad (24d)$$

$$\theta_R = \tan^{-1}(h/r_R), \quad \gamma_R = \frac{AP_R}{N_0}. \quad (24e)$$

and r_C^{rc} indicates the radius of the coverage area C for the relaying communication.

Proof: The proof is analogous to [20] and is given in Appendix D. ■

The relation in (24) shows that the relaying outage probability $\mathcal{P}_{\text{out}}^{\text{rc}}(r_D, h)$ exponentially decreases with the density of the relays λ . In the following corollary a lower bound for $\mathcal{P}_{\text{out}}^{\text{rc}}(r_D, h)$ simplifies the corresponding expression.

Corollary 2: The outage probability of the relaying communication in (24) is lower bounded as

$$\mathcal{P}_{\text{out}}^{\text{rc}}(r_D, h) \geq e^{-\lambda[\psi_{01} - \psi_{02}(r_D)]}, \quad (25)$$

where $\psi_{01} = |C|$ is the area of C , and

$$\begin{aligned} \psi_{02}(r_D) &= \int_0^{2\pi} \int_0^{r_C^{\text{rc}}} r_R \left[1 - Q\left(\sqrt{2\kappa_0}, \sqrt{2(\kappa_0 + 1)\xi\ell_{RD}^{\alpha_0}/\gamma_R}\right) \right] dr_R d\varphi_R. \\ & \quad (26) \end{aligned}$$

Proof: Assume that in the first phase all the relay nodes over C are able to decode the received signal from the UAV. In this case by denoting the outage probability as $\mathcal{P}_{\text{out}}^{\text{LB}}$ we have $\mathcal{P}_{\text{out}}^{\text{rc}} \geq \mathcal{P}_{\text{out}}^{\text{LB}}$. To compute $\mathcal{P}_{\text{out}}^{\text{LB}}$ we notice that the aforementioned assumption leads to $\lambda_{\mathcal{A}} = \lambda$ and hence

$$\mu_{\mathcal{A}} = \int_C \lambda_{\mathcal{A}} dC = \lambda|C|. \quad (27)$$

In addition (79) can be simplified to

$$\begin{aligned} \mathbb{P}(\Gamma_{RD} \leq \xi) &= \int_C \mathbb{P}(\Gamma_{RD} \leq \xi \mid \mathbf{R} : (r_R, \varphi_R)) \frac{\lambda}{\mu_{\mathcal{A}}} dC \\ & \quad (28a) \end{aligned}$$

$$= \frac{1}{|C|} \int_C \mathbb{P}\left(\frac{AP_R}{N_0 \ell_{RD}^{\alpha_0}} \Omega_{RD} \leq \xi \mid \mathbf{R} : (r_R, \varphi_R)\right) dC \quad (28b)$$

$$= \frac{1}{|C|} \int_0^{2\pi} \int_0^{r_C^{\text{rc}}} r_R \left[1 - Q\left(\sqrt{2\kappa_0}, \sqrt{2(\kappa_0 + 1)\xi\ell_{RD}^{\alpha_0}/\gamma_R}\right) \right] dr_R d\varphi_R. \quad (28c)$$

Therefore, by using (27) and (80) one obtains

$$\mathcal{P}_{\text{out}}^{\text{LB}} = e^{-\lambda[\psi_{01} - \psi_{02}(r_D)]}. \quad (29)$$

■
The proposed lower bound for $\mathcal{P}_{\text{out}}^{\text{rc}}$ can be reached at the altitudes of the UAV where it has a good channel condition only with the relay nodes in vicinity of the destination. This is due to the fact that the best relay in the second phase is more likely to be chosen among the candidates located near the destination enduring lower path loss. Therefore, although the mathematical solution for $\mathcal{P}_{\text{out}}^{\text{LB}}$ is based on the assumption that all the relay nodes successfully decode the UAV's signal in the first phase, considering the second phase of communication and the above-mentioned opportunistic relaying strategy, if only the relay nodes in the proximity of the destination successfully decode the transmitted signal the lower bound provides a tight approximation of the actual outage probability. This fact suggests a range of altitude at which the UAV can reach the lowest outage probability in relaying strategy. This is further explored in Section VI.

B. Cooperative Communication

In an opportunistic relaying cooperative network, the destination D receives the transmitted signal by the UAV from both the direct and the best relay path in the first and second phase respectively. Considering the selection combining strategy in which only the received signal with the highest SNR at the destination is selected, the total outage probability of the cooperative communication $\mathcal{P}_{\text{out}}^{\text{cc}}$ can be written as

$$\mathcal{P}_{\text{out}}^{\text{cc}} = \mathbb{P}(\max\{\Gamma_{\text{UD}}, \Gamma_{\text{R,D}}\} \leq \xi) = \mathcal{P}_{\text{out}}^{\text{dc}} \cdot \mathcal{P}_{\text{out}}^{\text{rc}}, \quad (30)$$

where the last equation is due to the independency of fading between any pair of nodes. By substituting $\mathcal{P}_{\text{out}}^{\text{dc}}$ and $\mathcal{P}_{\text{out}}^{\text{rc}}$ from (8) and (24) into (30) the total outage probability is obtained, which is a function of r_{D} and h , i.e. $\mathcal{P}_{\text{out}}^{\text{cc}} = \mathcal{P}_{\text{out}}^{\text{cc}}(r_{\text{D}}, h)$. Note that in (24) $\tilde{r}_{\text{C}}^{\text{rc}}$ is to be replaced with $\tilde{r}_{\text{C}}^{\text{cc}}$ which is the radius of C for cooperative communication.

Due to the complicated expressions of $\mathcal{P}_{\text{out}}^{\text{rc}}$ and $\mathcal{P}_{\text{out}}^{\text{cc}}$ in (24) and (30), the problems (5) and (7) for relaying and cooperative communication are not mathematically tractable. However, numerical optimization for particular scenarios is possible. An example of this is presented in Section VI-B.

VI. CASE STUDY: A PARTICULAR DEPENDENCY FOR α AND K OVER θ

In this section we propose specific relations for $\alpha(\theta)$ and $K(\theta)$ needed for numerical results.

A. Models for $\alpha(\theta)$ and $K(\theta)$

The value of path loss exponent is typically proportional to the density of obstacles between the transmitter and receiver such that a larger α is assumed in denser areas. Therefore, $\alpha(\theta)$ can be characterized using the notion of probability of line of sight (LoS) $\mathcal{P}_{\text{LoS}}(\theta)$ between the UAV and the ground node [15]. This relationship is defined as

$$\alpha(\theta) = a_1 \cdot \mathcal{P}_{\text{LoS}}(\theta) + b_1, \quad (31)$$

where ³

$$\mathcal{P}_{\text{LoS}}(\theta) = \frac{1}{1 + a_2 e^{-b_2 \theta}}, \quad (32)$$

and a_1 , b_1 , a_2 and b_2 are determined by the environment characteristics and the transmission frequency, and θ is in radian. A direct calculation shows that

$$\begin{aligned} a_1 &= \frac{\alpha_{\frac{\pi}{2}} - \alpha_0}{\mathcal{P}_{\text{LoS}}(\frac{\pi}{2}) - \mathcal{P}_{\text{LoS}}(0)} \cong \alpha_{\frac{\pi}{2}} - \alpha_0, \\ b_1 &= \alpha_0 - a_1 \cdot \mathcal{P}_{\text{LoS}}(0) \cong \alpha_0, \end{aligned} \quad (33)$$

where the approximations are due to the fact that $\mathcal{P}_{\text{LoS}}(0) \rightarrow 0$ and $\mathcal{P}_{\text{LoS}}(\frac{\pi}{2}) \rightarrow 1$. The proposed model for $\alpha(\theta)$ in (31) is further discussed relying on the recent reports in Appendix E.

For the Rician factor, in consistency with [33], we follow the exponential dependency between K and θ as

$$K(\theta) = a_3 \cdot e^{b_3 \theta}, \quad (34)$$

³The LoS probability is generally dependent on the height of a transmitter, the height of the receiver and the ground distance between them. However, an approximation in [15] shows that for an A2G communication link \mathcal{P}_{LoS} can be simplified only as a function of the elevation angle.

where θ is in radian and a_3 and b_3 are environment and frequency dependent constant parameters which are related to κ_0 and $\kappa_{\pi/2}$ as

$$a_3 = \kappa_0, \quad b_3 = \frac{2}{\pi} \ln \left(\frac{\kappa_{\frac{\pi}{2}}}{\kappa_0} \right). \quad (35)$$

Note that the general shape of $\alpha(\theta)$ and $K(\theta)$ can change over different environments and system parameters that could be specified by the measurements in concrete scenarios.

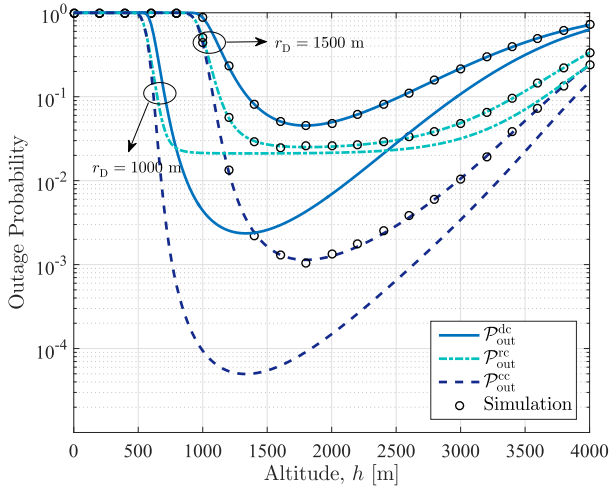
B. Simulation and Discussion

In this section the simulations are provided to discuss the analytical results obtained in the previous sections.

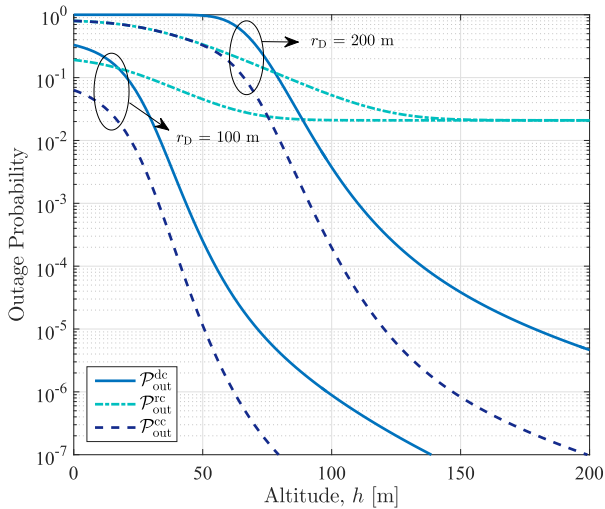
1) *Without Power Optimization*: The parameters used in this subsection are set to $\gamma_{\text{U}} = \gamma_{\text{R}} = 75$ dB, $\kappa_0 = 5$ dB, $\kappa_{\frac{\pi}{2}} = 15$ dB, $\alpha_0 = 3.5$, $\alpha_{\frac{\pi}{2}} = 2$, and $\lambda = 0.0003$, unless otherwise indicated.

Figure 3a shows that the analytical results of the outage probability are in a good conformity with the simulation results for each of direct, relaying and cooperative communication in which 10^5 independent network realizations are employed for the simulations. As can be seen from Figures 3a and 3b, comparing with G2G communication, i.e. $h = 0$, the outage performance is significantly enhanced by exploiting UAV at an appropriate altitude which depends on the distance r_{D} . Moreover, the existence of altitudes $\hat{h}^{\text{Y}} = \hat{h}_{\text{D}}^{\text{dc}}, \hat{h}_{\text{D}}^{\text{rc}}, \hat{h}_{\text{D}}^{\text{cc}}$, or the corresponding elevation angles $\hat{\theta}_{\text{D}}^{\text{Y}} = \hat{\theta}_{\text{D}}^{\text{dc}}, \hat{\theta}_{\text{D}}^{\text{rc}}, \hat{\theta}_{\text{D}}^{\text{cc}}$ can be observed from Figure 3a, where the outage probabilities are minimized. In fact for $h < \hat{h}^{\text{Y}}$ the benefits of the reduced path loss exponent α and the increased Rician factor K with increasing h becomes more significant than the losses caused by the increased link length and hence the outage probability decreases. However beyond \hat{h}^{Y} the impact of the link length dominates the other factors and hence leads to an increased outage probability. Therefore, at $h = \hat{h}^{\text{Y}}$ the impact of the above-mentioned factors are balanced resulting in the minimum outage probability. This altitude increases with the distance r_{D} as can be seen in the figure.

Is interesting to note that, according to Figure 3a, the relaying communication outage probability $\mathcal{P}_{\text{out}}^{\text{rc}}$ might be lower or higher than that of the direct communication $\mathcal{P}_{\text{out}}^{\text{dc}}$ depending on the altitude h and the destination distance r_{D} . For instance at $r_{\text{D}} = 1000$ m, $\mathcal{P}_{\text{out}}^{\text{rc}}$ is bigger than $\mathcal{P}_{\text{out}}^{\text{dc}}$ at very low and very high altitudes, however for moderate altitudes the direct communication performs better than the relaying communication. Indeed, the relaying outage probability is limited by the second phase of the corresponding communication strategy where G2G link endures a larger path loss exponent. Due to this fact, $\mathcal{P}_{\text{out}}^{\text{rc}}$ remains approximately constant over a range of UAV's altitude at which the A2G link has a good quality and hence the overall relaying outage performance is determined by the G2G link. Therefore, the outage probability of cooperative communication $\mathcal{P}_{\text{out}}^{\text{cc}}$, which is the product of $\mathcal{P}_{\text{out}}^{\text{dc}}$ and $\mathcal{P}_{\text{out}}^{\text{rc}}$, is minimized approximately at the altitude of the UAV where $\mathcal{P}_{\text{out}}^{\text{dc}}$ reaches its minimum. In other words $\hat{h}_{\text{D}}^{\text{dc}} \cong \hat{h}_{\text{D}}^{\text{cc}}$ and hence $\hat{\theta}_{\text{D}}^{\text{dc}} \cong \hat{\theta}_{\text{D}}^{\text{cc}}$. This fact is illustrated in Figure 4.



(a)



(b)

Fig. 3. (a) The optimal altitude for the minimum outage probability is mainly determined by $\mathcal{P}_{\text{out}}^{\text{dc}}$. Because of the low transmit power considered in this simulation, the outage probability at low altitudes is very high, yet when optimizing the altitude we can achieve a very good outage performance with the same transmit power. (b) The impact of low altitudes is more significant for shorter distances.

The values of $\tilde{\theta}_D^{\text{dc}}$ obtained from Theorem 1 are compared with the exact (numerical) values in Figure 4 which shows the accuracy of the analytical solution proposed in the theorem. As can be seen, $\tilde{\theta}_D^{\text{dc}}$ reduces with r_D since the link length is more susceptible to the elevation angle at larger r_D and hence the beneficial effect of reduction in α and increase in K becomes less noticeable compared to the additional link length. However $\tilde{\theta}_D^{\text{dc}}$ is approximately independent from r_D at larger distances. According to Figure 4, although $\tilde{\theta}_D^{\text{rc}}$ may be different with $\tilde{\theta}_D^{\text{dc}}$ at low altitudes, $\tilde{\theta}_D^{\text{cc}}$ is equal to $\tilde{\theta}_D^{\text{dc}}$ which means that the equation (11) is valid for cooperative communication as well. In fact, the best relay location is mainly determined in the second phase since the candidate relays in the neighborhood of the destination have quality LoS links with the UAV in the first phase. On the other hand, in the second phase the closer relays to the destination are

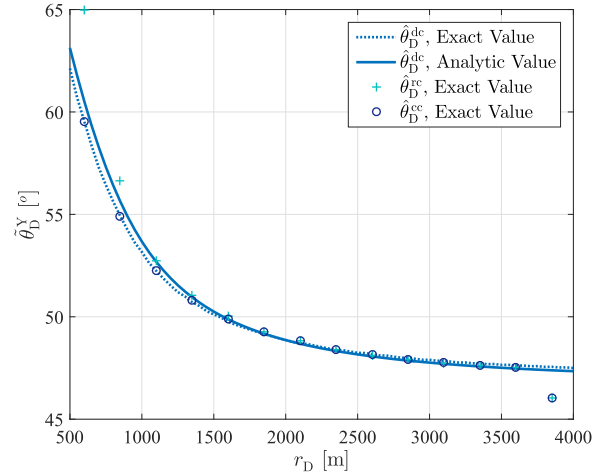


Fig. 4. The analytical solution for $\tilde{\theta}_D^{\text{dc}}$ closely matches the value obtained by the numerical simulation. Moreover, $\tilde{\theta}_D^{\text{cc}}$ is mainly determined by the direct communication link such that $\tilde{\theta}_D^{\text{cc}} = \tilde{\theta}_D^{\text{dc}}$ except near the border of \mathcal{C} .

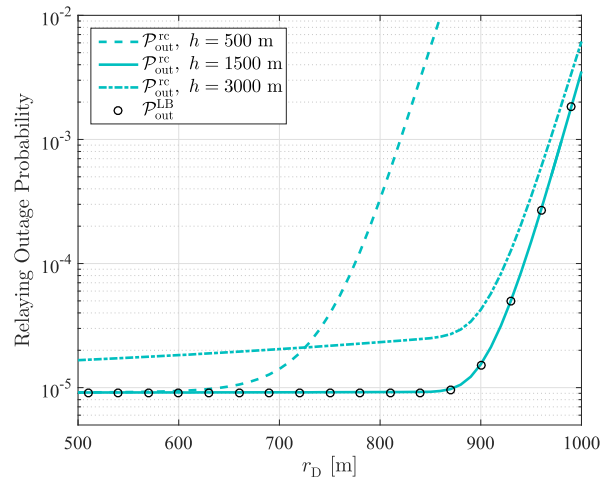


Fig. 5. The proposed lower bound outage probability $\mathcal{P}_{\text{out}}^{\text{LB}}$ is very tight over the entire range of r_D when the UAV is in appropriate altitudes.

more likely to be chosen as the best relay, which are in a random location around the destination with a larger or smaller elevation angle compared to that of destination. Therefore, on average the optimum elevation angle of the best relay is such that $\tilde{\theta}_D^{\text{rc}}$ remains the same as $\tilde{\theta}_D^{\text{dc}}$. However, close to the border of \mathcal{C} , both $\tilde{\theta}_D^{\text{rc}}$ and $\tilde{\theta}_D^{\text{cc}}$ deviate from $\tilde{\theta}_D^{\text{dc}}$ owing to the fact that the candidate relays for cooperation are limited to the region between the UAV and the destination D and hence the elevation angle for minimum outage probability decreases.

Figure 5 shows that the proposed lower bound for relaying communication is tight over the entire range of r_D at the optimal altitudes. This is due to the fact that the relay nodes around the neighboring of destination are well connected to the UAV and thus the outage event only occurs in the second phase of relaying communication. The tightness of lower bound outage probability enables us to use it instead of the complex exact expression for $\mathcal{P}_{\text{out}}^{\text{rc}}$ obtained in the previous section.

The locus of the configuration space \mathcal{S}^Y for $Y = \text{dc}, \text{rc}, \text{cc}$ are depicted in Figure 6. As can be seen, the impact of third dimension, i.e. altitude, by exploiting UAV is striking in

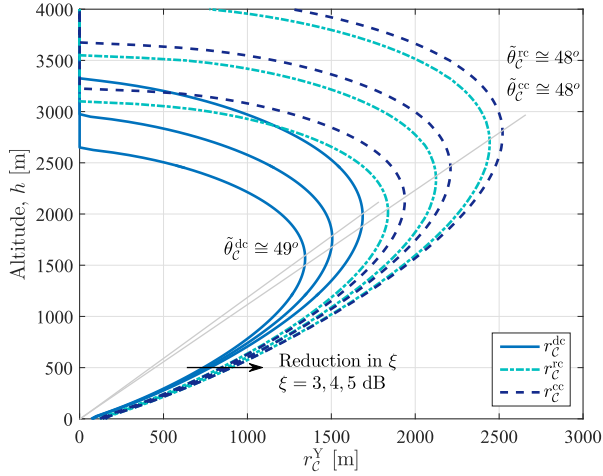


Fig. 6. Configuration space S^Y for different type of communications. The optimum elevation angle $\tilde{\theta}_C^Y$ is independent of the SNR requirement ξ .

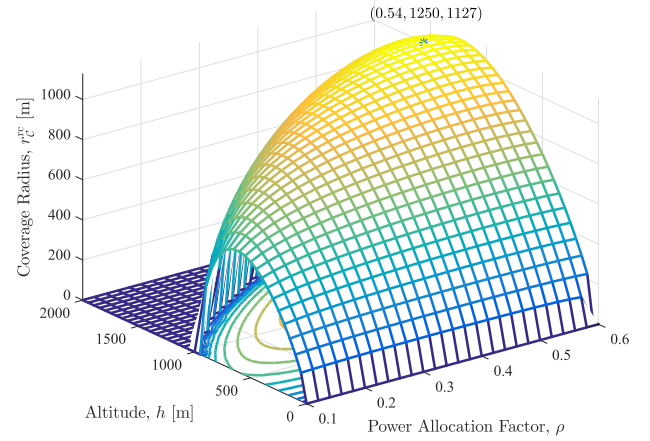
order to extend the coverage range. Furthermore, there exists an optimum altitude \tilde{h}_C^Y and elevation angle $\tilde{\theta}_C^Y$ which leads to the maximum coverage radius \tilde{r}_C^Y . The figure shows that $\tilde{\theta}_C^Y$ is independent of the SNR requirement ξ and hence the ratio of $\tilde{h}_C^Y/\tilde{r}_C^Y$ is constant. However, \tilde{h}_C^Y and $\tilde{\theta}_C^Y$ diminish with ξ as expressed in (21). Figure 6 also shows that the relaying communication might finally result in a coverage area larger than that of direct communication, although $\mathcal{P}_{\text{out}}^{\text{rc}}$ is higher than $\mathcal{P}_{\text{out}}^{\text{dc}}$ at some altitudes h and distances r_D which can be seen in Figure 3a.

2) *Power Allocation for Maximum Coverage*: One of the main advantages of cooperative communication technique is an improvement in network efficiency by appropriately distributing the transmitted power throughout the nodes. In this subsection we study the optimal height-dependent power allocation strategy for maximum coverage. In fact, we assume a total power budget of P_T and hence we assign $P_U = P_T$ for direct communication and $P_U + P_R = P_T$ for relaying and cooperative communication. The fundamental concern here is how the power budget is to be assigned to each of the transmitting nodes in order to increase the coverage range. To this end, we define the power allocation factor ρ as

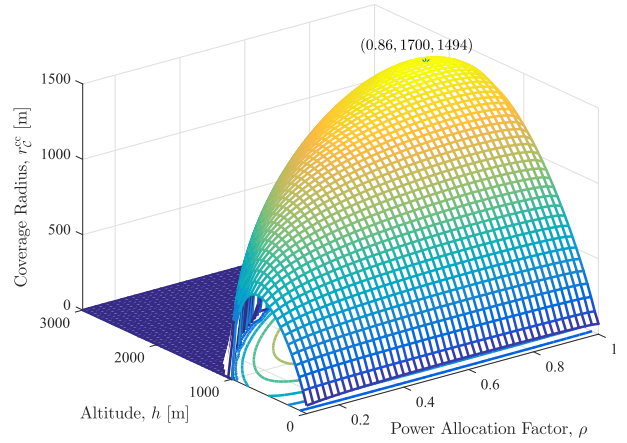
$$\rho = \frac{P_U}{P_U + P_R}, \quad (36)$$

representing the portion of power budget allocated to the UAV. Therefore, in the following we discuss the maximum coverage obtained by using the optimum ρ in each altitude. The optimum power allocation factor for relaying and cooperative strategy are denoted as $\tilde{\rho}_C^{\text{rc}}$ and $\tilde{\rho}_C^{\text{cc}}$ respectively. Please note that this study also enables us to provide a fair comparison between direct and cooperative communication by adopting the same total transmit power budget at the transmitting nodes.

Figures 7 shows that the coverage radius is a concave function of power allocation factor ρ at each altitude which results in an optimum ρ maximizing the coverage. This means that the performance of the network is maximized when the available power budget is optimally assigned to each of two phases. The same behavior can be observed while looking at coverage radius as function of altitude for a given ρ . This fact



(a)



(b)

Fig. 7. (a) The coverage radius is maximized at the optimum altitude by allocating the optimum portion of transmission power budget to the UAV. (b) The optimum power allocation factor in cooperative communication is larger than that of the relaying strategy.

leads to a unique optimum h and ρ for the maximum coverage radius as is marked in the figures. Generally speaking, at each altitude, allocating more power to the UAV is more effective than to the relays since the communication channel between the UAV and a ground terminal suffers from less path loss than a channel between a relay and a ground destination D , and hence $\tilde{\rho}_C^{\text{rc}} > 0.5$. The optimum power allocation factor for cooperative communication, i.e. $\tilde{\rho}_C^{\text{cc}}$, is even larger than $\tilde{\rho}_C^{\text{rc}}$ since the UAV's signal is also received at the destination which increases the contribution of UAV's transmit power to the final received SNR and hence to the coverage radius.

Figure 8a shows the coverage radius of the UAV at each altitude while employing the optimum ρ . As can be seen, depending on the density of relays, r_C^{rc} could be larger than r_C^{dc} even though the UAV transmit power is lower. Therefore, the relaying strategy might perform better than the direct communication while adopting the same overall transmit power budget. Moreover, cooperative communication always results in a larger coverage area independent from the density of relays λ . This is due to the fact that the portion of relaying

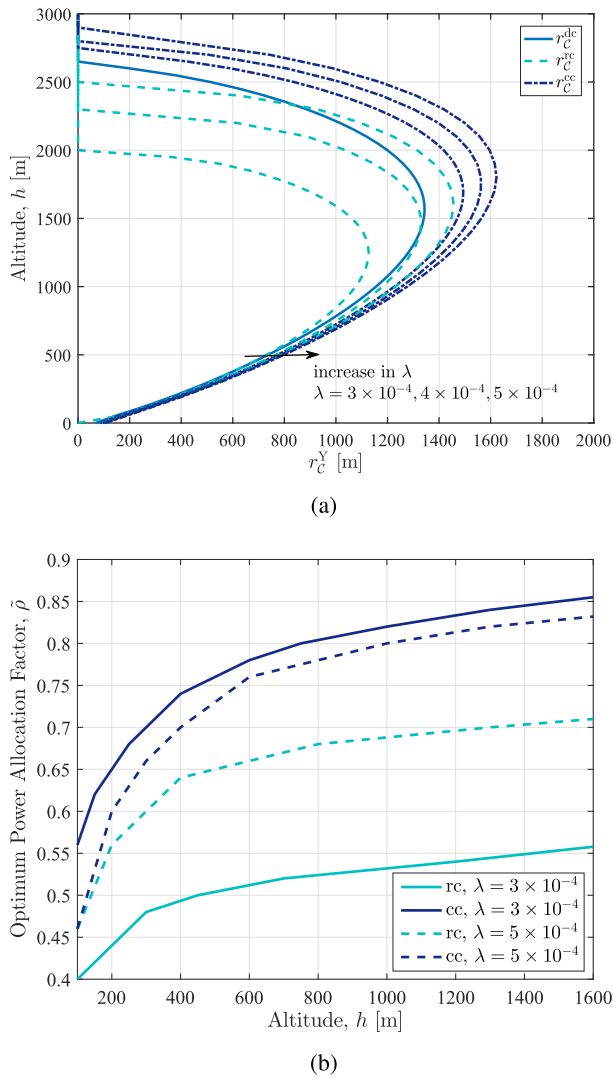


Fig. 8. (a) Even using the same transmission power budget, cooperative communication results in a larger coverage area. (b) Optimum ratio of power allocation $\tilde{\rho}_C$ increases with altitude h . It is interesting to see that for lower altitude (which is the realistic region given regulatory constraints that limit UAVs to fly too high), the optimal power allocation strategy gives less power to the UAV. This is good, as this means that the power requirement for those low altitude UAVs is lower, however, means also that a ground relay communication strategy is important.

transmit power is determined based on the availability of the relay nodes such that for denser areas more power is dedicated to the relays and hence optimal ρ decreases as λ increases (see Figure 8b). However, for relaying communication optimal ρ grows as λ becomes larger. As is shown in Figure 8b, the optimum power allocation factors, i.e. $\tilde{\rho}_C^{rc}$ and $\tilde{\rho}_C^{cc}$, are an increasing function of altitude h . Therefore, as the UAV goes higher more portion of power budget is to be assigned to the UAV for maximum coverage range.

VII. CONCLUSION

The analysis of UAV networks requires a detailed model of the A2G communication links as function of distance and height. A generic A2G analytical framework was proposed, which takes into account the dependence of the path loss

exponent and multipath fading on the height and angle of the UAV. We showed how this model enables a characterization of the performance and reliability of A2G cooperative communication networks.

Moreover, the model enables to derive the UAV altitude that maximizes the reliability and coverage range, which is crucial for UAV usage scenarios such as aerial sensing or data streaming. Results show that the optimal altitude for maximum reliability is mainly determined by the direct link of communication in an A2G cooperative system, as the relaying communication achieves a stable performance for a wide range of UAV altitudes. For a specific scenario with a communication range of 1000m with a low transmit power, the optimal UAV altitude was shown to be 1300m for the direct communication, while a range of 700m to 2000m approximated the optimal UAV altitude for the relaying communication.

Furthermore, by constraining the total transmit power budget, our results give insight in the dimensioning of the system. For example, for a UAV altitude of 200m that complies with regulatory constraints, our analysis shows that an allocation of 35% lower transmit power to the UAV, it is possible to obtain the same coverage range, thanks to the inclusion of ground relays. Alternatively, if in a similar scenario the UAV height is unconstrained, the coverage range increases up to 25% compared to the direct communication at the optimum altitudes yet with even 15% lower UAV transmit power. In fact, this reduction of the UAVs transmit power is of practical importance, first because of the limitation in the source of UAVs power. Second, the UAVs due to the higher LoS probability impose more interference to the ground users compared to the terrestrial interferers and hence their transmit power is to be lowered. This fact will be more investigated in our future study. We will also use the results of this paper as a basis to optimize a network of multiple UAV base stations.

APPENDIX A

PROOF OF THEOREM 1

For the elevation angle of the UAV $\hat{\theta}_D^{dc}$ at which the link's outage probability $\mathcal{P}_{out}^{dc}(r_D, h)$ is minimized, one can write

$$\frac{\partial}{\partial \theta_D} \mathcal{P}_{out}^{dc}(r_D, h) = 0. \quad (37)$$

By defining the auxiliary variables x and y as

$$x = \sqrt{2K(\theta_D)}, \quad y = \sqrt{2\zeta [1 + K(\theta_D)] \ell_{UD}^{\alpha(\theta_D)} / \gamma_U}, \quad (38)$$

which are the first and second arguments of the Marcum Q-function in (8) respectively, and replacing $\mathcal{P}_{out}^{dc}(r_D, h)$ from (8) into (37) we have

$$0 = \frac{\partial}{\partial \theta_D} Q(x, y) = \frac{\partial Q(x, y)}{\partial x} \cdot \frac{\partial x}{\partial \theta_D} + \frac{\partial Q(x, y)}{\partial y} \cdot \frac{\partial y}{\partial \theta_D}, \quad (39)$$

where the last equation is obtained following multivariable chain rule differentiation. From [34] one sees that

$$\begin{aligned} \frac{\partial Q(x, y)}{\partial x} &= y e^{-\frac{x^2+y^2}{2}} I_1(xy), \\ \frac{\partial Q(x, y)}{\partial y} &= -y e^{-\frac{x^2+y^2}{2}} I_0(xy). \end{aligned} \quad (40)$$

Substituting (40) into (39) yields

$$y e^{-\frac{x^2+y^2}{2}} I_1(xy) \cdot \frac{\partial x}{\partial \theta_D} - y e^{-\frac{x^2+y^2}{2}} I_0(xy) \cdot \frac{\partial y}{\partial \theta_D} = 0, \quad (41)$$

or equivalently

$$\frac{\partial y}{\partial \theta_D} = \frac{I_1(xy)}{I_0(xy)} \cdot \frac{\partial x}{\partial \theta_D}. \quad (42)$$

Using (38) one can write

$$\frac{\partial x}{\partial \theta_D} = \frac{K'(\theta_D)}{\sqrt{2K(\theta_D)}} = \frac{K'(\theta_D)}{x}, \quad (43)$$

where $K'(\cdot)$ indicates the derivative function of $K(\cdot)$. In order to compute the derivative of y with respect to θ_D in (38) we notice that $\ell_{UD} = r_D / \cos(\theta_D)$. Thus we can write

$$\ln(y) = \frac{1}{2} \left[\ln \left(\frac{2\xi}{\gamma U} \right) + \ln[1 + K(\theta_D)] + \alpha(\theta_D) \ln \left(\frac{r_D}{\cos(\theta_D)} \right) \right]. \quad (44)$$

Taking the derivative with respect to θ_D in the above equation yields

$$\frac{\partial y}{\partial \theta_D} = \frac{y}{2} \left[\frac{K'(\theta_D)}{1 + K(\theta_D)} + \alpha'(\theta_D) \ln \left(\frac{r_D}{\cos(\theta_D)} \right) + \alpha(\theta_D) \tan(\theta_D) \right] \quad (45)$$

or equivalently

$$\frac{\partial y}{\partial \theta_D} = \frac{y}{2} \left[\frac{K'(\theta_D)}{1 + K(\theta_D)} + \alpha'(\theta_D) \ln \left(\frac{r_D}{\cos(\theta_D)} \right) + \alpha(\theta_D) \tan(\theta_D) \right]. \quad (46)$$

By using (42), (43) and (46) one can write

$$\begin{aligned} \frac{xy}{2} \left[\frac{K'(\theta_D)}{1 + K(\theta_D)} + \alpha'(\theta_D) \ln \left(\frac{r_D}{\cos(\theta_D)} \right) + \alpha(\theta_D) \tan(\theta_D) \right] \\ = \frac{I_1(xy)}{I_0(xy)} K'(\theta_D). \end{aligned} \quad (47)$$

Now assuming that xy at $\theta_D = \tilde{\theta}_D^{\text{dc}}$ is large enough, we use the following approximation [35]

$$\frac{I_1(xy)}{I_0(xy)} = 1 - \frac{1}{2xy} - \frac{1}{8(xy)^2} + \mathcal{O}[(xy)^{-3}] \cong 1. \quad (48)$$

On the other hand, assuming that $K(\tilde{\theta}_D^{\text{dc}}) \gg 1$, from (38) one obtains

$$xy \cong 2K(\theta_D) \sqrt{\frac{\xi}{\gamma U} \left[\frac{r_D}{\cos(\theta_D)} \right]^{\alpha(\theta_D)}}. \quad (49)$$

Therefore, from (47), (48) and (49) and using the assumption of $K(\tilde{\theta}_D^{\text{dc}}) \gg 1$ we finally obtain

$$\begin{aligned} \sqrt{\frac{\xi}{\gamma U} \left[\frac{r_D}{\cos(\theta_D)} \right]^{\alpha(\theta_D)}} \left[\frac{K'(\theta_D)}{K(\theta_D)} + \alpha'(\theta_D) \ln \left(\frac{r_D}{\cos(\theta_D)} \right) \right. \\ \left. + \alpha(\theta_D) \tan(\theta_D) \right] = \frac{K'(\theta_D)}{K(\theta_D)}. \end{aligned} \quad (50)$$

APPENDIX B

PROOF OF LEMMA 1

Rewriting $y = Q^{-1}(x, 1 - \varepsilon)$ as

$$Q(x, y) = 1 - \varepsilon, \quad (51)$$

and taking its derivative with respect to x yields

$$\frac{\partial Q(x, y)}{\partial x} + \frac{\partial Q(x, y)}{\partial y} \frac{dy}{dx} = 0. \quad (52)$$

By using (40) in (52) one obtains

$$y e^{-\frac{x^2+y^2}{2}} I_1(xy) - y e^{-\frac{x^2+y^2}{2}} I_0(xy) \frac{dy}{dx} = 0 \quad (53)$$

or equivalently

$$\frac{dy}{dx} = \frac{I_1(xy)}{I_0(xy)}. \quad (54)$$

For small x we have [35]

$$I_n(xy) \cong \left(\frac{xy}{2} \right)^n; \quad n = 0, 1. \quad (55)$$

Thus (54) can be rewritten as $\frac{dy}{dx} = \frac{xy}{2}$ which is a first order differential equation with the solution of

$$y = y_0 e^{\frac{x^2}{4}}, \quad (56)$$

where y_0 is the value of y at $x = 0$. In order to find y_0 we notice that $Q(0, y_0) = 1 - \varepsilon$ and from [34] one sees that $Q(0, y_0) = e^{-\frac{y_0^2}{2}}$. Thus, we have

$$y_0 = \sqrt{-2 \ln(1 - \varepsilon)}. \quad (57)$$

For the large values of x from (48) one can write $\frac{I_1(xy)}{I_0(xy)} \cong 1 - \frac{1}{2xy}$ which can be used in (54) to yield

$$\frac{dy}{dx} \cong 1 - \frac{1}{2xy}. \quad (58)$$

In order to solve the above differential equation first we solve the equation by neglecting $1/2xy$. To this end, we rewrite it as $\frac{dy}{dx} \cong 1$. This equation has a simple solution as

$$y \cong x + \eta_{1\varepsilon}, \quad (59)$$

where $\eta_{1\varepsilon}$ is a constant determined by ε . Now by using $y = x + \eta_{1\varepsilon}$, the equation (58) can be rewritten as

$$\frac{dy}{dx} \cong 1 - \frac{1}{2x(x + \eta_{1\varepsilon})} = 1 - \frac{1}{2\eta_{1\varepsilon}} \left[\frac{1}{x} - \frac{1}{x + \eta_{1\varepsilon}} \right]. \quad (60)$$

Therefore, taking the integral of the above equation obtains

$$\begin{aligned} y &\cong x - \frac{1}{2\eta_{1\varepsilon}} [\ln(x) - \ln(x + \eta_{1\varepsilon})] + \eta_{2\varepsilon} \\ &= x - \frac{1}{2\eta_{1\varepsilon}} \ln \left[\frac{x}{x + \eta_{1\varepsilon}} \right] + \eta_{2\varepsilon}. \end{aligned} \quad (61)$$

It is to be noted that as $x \rightarrow \infty$, from (61) one finds $y = x + \eta_{2\varepsilon}$ where in comparison with (59) results in $\eta_{2\varepsilon} = \eta_{1\varepsilon} \triangleq \eta_\varepsilon$. In conclusion (61) can be rewritten as

$$y \cong x - \frac{1}{2\eta_\varepsilon} \ln \left[\frac{x}{x + \eta_\varepsilon} \right] + \eta_\varepsilon. \quad (62)$$

To obtain η_ε one can find that $x \rightarrow \infty$ leads to $y = x + \eta_\varepsilon$ which means that $y \rightarrow \infty$ and $y \gg y - x$. On the other hand, from [36] the conditions $y \rightarrow \infty$ and $y \gg y - x$ results in $Q(x, y) = Q(y - x)$. Thus, since $1 - \varepsilon = Q(x, y)$ we have $1 - \varepsilon = Q(y - x) = 1 - Q(x - y)$ or $Q(x - y) = \varepsilon$. Therefore $Q(-\eta_\varepsilon) = \varepsilon$ or $\eta_\varepsilon = -Q^{-1}(\varepsilon)$.

Note that if $Q^{-1}(\varepsilon) = 0$ the relation in (62) is ambiguous. To resolve this issue, we re-compute y from (60) by replacing $\eta_{1\varepsilon} = 0$. Thus, we have $\frac{dy}{dx} \cong 1 - \frac{1}{2x^2}$ which results in

$$y \cong x + \frac{1}{2x} + \eta_\varepsilon, \quad (63)$$

where $\eta_\varepsilon = -Q^{-1}(\varepsilon)$ as explained before.

In conclusion, from (56), (57), (62) and (63) for $Q^{-1}(\varepsilon) \neq 0$ we obtain

$$y = \begin{cases} \sqrt{-2 \ln(1 - \varepsilon)} e^{\frac{x^2}{4}}; & x \leq x_0 \\ x - \frac{1}{2\eta_\varepsilon} \ln\left(\frac{x}{x + \eta_\varepsilon}\right) + \eta_\varepsilon; & x > x_0 \wedge \eta_\varepsilon = -Q^{-1}(\varepsilon) \end{cases} \quad (64)$$

and for $Q^{-1}(\varepsilon) = 0$ we have

$$y = \begin{cases} \sqrt{-2 \ln(1 - \varepsilon)} e^{\frac{x^2}{4}}; & x \leq x_0 \\ x + \frac{1}{2x}; & x > x_0 \end{cases} \quad (65)$$

where x_0 can be determined by the intersection of the sub-functions at $x > \max[0, Q^{-1}(\varepsilon)]$. To clarify this, we note that $y = \sqrt{-2 \ln(1 - \varepsilon)} e^{x^2/4}$ is an strictly increasing function which goes away from $Q^{-1}(x, 1 - \varepsilon)$ to $+\infty$ at $x \geq \max[0, Q^{-1}(\varepsilon)]$, whereas $y = x - \frac{1}{2\eta_\varepsilon} \ln\left(\frac{x}{x + \eta_\varepsilon}\right) + \eta_\varepsilon$ sharply decreases from $+\infty$ to $Q^{-1}(x, 1 - \varepsilon)$ since $\ln[x/(x + \eta_\varepsilon)]$ is dominant term at the vicinity of $\max[0, Q^{-1}(\varepsilon)]$. Considering this fact, at a unique x_0 these two sub-functions meet each other which is considered as the decision point to switch the approximate values for $y = Q^{-1}(x, 1 - \varepsilon)$ based on the proposed piecewise function. According to the above discussion, at $x = x_0$ the piecewise function returns the least accurate approximation. The same argument is used for finding the value of x_0 in (65).

Figure 9 compares the proposed analytic solution for $y = Q^{-1}(x, 1 - \varepsilon)$ with the exact values. As can be seen, the analytic solution is a good approximate of the exact values.

APPENDIX C PROOF OF THEOREM 3

The derivative of the coverage radius r_C^{dc} at its maximum should be zero. Thus

$$\frac{\partial}{\partial \theta_C} r_C^{\text{dc}} = 0 \quad (66)$$

or equivalently

$$\frac{\partial}{\partial \theta_C} \ln(r_C^{\text{dc}}) = 0. \quad (67)$$

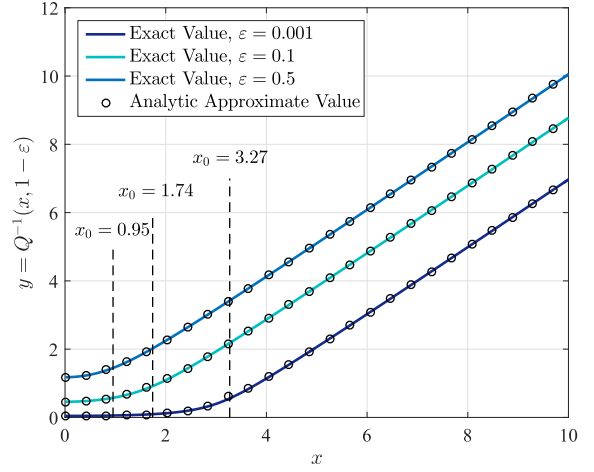


Fig. 9. The proposed analytic solution for $y = Q^{-1}(x, 1 - \varepsilon)$ is a good approximation of the exact value.

From (13b) one obtains $\ln(r_C^{\text{dc}}) = \ln[\Lambda(\theta_C)] + \ln[\cos(\theta_C)]$ and hence by taking the derivative

$$\begin{aligned} \frac{\partial}{\partial \theta_C} \ln(r_C^{\text{dc}}) &= \frac{\partial}{\partial \theta_C} \ln[\Lambda(\theta_C)] + \frac{\partial}{\partial \theta_C} \ln[\cos(\theta_C)] \\ &= \frac{\partial}{\partial \theta_C} \ln[\Lambda(\theta_C)] - \tan(\theta_C). \end{aligned} \quad (68a)$$

Replacing (13b) into (67) yields

$$\tan(\theta_C) = \frac{\partial}{\partial \theta_C} \ln[\Lambda(\theta_C)]. \quad (69)$$

Assuming $x_C \gg \sqrt{2}$ at $\theta_C = \tilde{\theta}_C^{\text{dc}}$, we can simplify $\Lambda(\theta_C)$ in (13c) as

$$\Lambda(\theta_C) \cong \left(\frac{\gamma_U y_C^2}{\xi x_C^2} \right)^{\frac{1}{\alpha(\theta_C)}}, \quad (70)$$

and y_C in (13d) as

$$y_C \cong x_C - Q^{-1}(\varepsilon). \quad (71)$$

Using (69) – (71) one can write

$$\begin{aligned} \tan(\theta_C) &= \frac{\partial}{\partial \theta_C} \left[\frac{\ln(\gamma_U/\xi) + 2 \ln(y_C) - 2 \ln(x_C)}{\alpha(\theta_C)} \right] \end{aligned} \quad (72a)$$

$$= \frac{\partial}{\partial \theta_C} \left[\frac{\ln(\gamma_U/\xi) + 2 \ln[x_C - Q^{-1}(\varepsilon)] - 2 \ln(x_C)}{\alpha(\theta_C)} \right] \quad (72b)$$

$$= \frac{2x'_C \left(\frac{1}{x_C - Q^{-1}(\varepsilon)} - \frac{1}{x_C} \right) \alpha(\theta_C) - \alpha'(\theta_C) \alpha(\theta_C) \ln[\Lambda(\theta_C)]}{\alpha(\theta_C)^2} \quad (72c)$$

$$= \frac{2x'_C \left(\frac{Q^{-1}(\varepsilon)}{x_C[x_C - Q^{-1}(\varepsilon)]} \right) - \alpha'(\theta_C) \ln[\Lambda(\theta_C)]}{\alpha(\theta_C)}, \quad (72d)$$

where in (72b) and (72c) the relations (71) and (70) are used respectively. The equation (72d) can be rewritten as

$$\begin{aligned} \alpha(\theta_C) \tan(\theta_C) + \alpha'(\theta_C) \ln[\Lambda(\theta_C)] \\ = 2x'_C \left(\frac{Q^{-1}(\varepsilon)}{x_C[x_C - Q^{-1}(\varepsilon)]} \right), \end{aligned} \quad (73)$$

which is the desired result.

APPENDIX D
PROOF OF THEOREM 4

Using the total probability theorem, (23) can be written as

$$\mathcal{P}_{\text{out}}^{\text{rc}} = \sum_{i=0}^{\infty} \mathbb{P}(\Gamma_{\text{R}_j\text{D}} \leq \zeta \mid |\mathcal{A}| = i) \mathbb{P}(|\mathcal{A}| = i) \quad (74)$$

where $|\mathcal{A}|$ indicates the cardinality of \mathcal{A} . Using Marking Theorem [37], \mathcal{A} follows PPP with the density obtained as

$$\lambda_{\mathcal{A}}(r_{\text{R}}, \varphi_{\text{R}}, h) = \lambda \mathbb{P}(\text{R} \in \mathcal{A}) = \lambda \mathbb{P}(\Gamma_{\text{UR}} > \zeta) \quad (75a)$$

$$= \lambda \mathbb{P}\left(\frac{AP_{\text{U}}}{N_0 \ell_{\text{UR}}^{\alpha(\theta_{\text{R}})}} \Omega_{\text{UR}} > \zeta\right) \quad (75b)$$

$$= \lambda Q\left(\sqrt{2K(\theta_{\text{R}})}, \sqrt{2[K(\theta_{\text{R}}) + 1]\zeta \ell_{\text{UR}}^{\alpha(\theta_{\text{R}})}/\gamma_{\text{U}}}\right), \quad (75c)$$

where $\theta_{\text{R}} = \tan^{-1}(h/r_{\text{R}})$, R is a relay node at an arbitrary location indicated by $(r_{\text{R}}, \varphi_{\text{R}})$ in polar coordinates, (75b) is obtained using (1) by replacing X with R , and (75c) follows from the fact that Ω_{UR} has a non-central chi-square PDF expressed in (2) with unit mean. Therefore, $|\mathcal{A}|$ is a Poisson random variable with mean $\mu_{\mathcal{A}}$ computed as

$$\begin{aligned} \mu_{\mathcal{A}}(h) &= \int_{\mathcal{C}} \lambda_{\mathcal{A}}(r_{\text{R}}, \varphi_{\text{R}}, h) d\mathcal{C} \\ &= 2\pi \lambda \int_0^{r_{\text{C}}^{\text{rc}}} r_{\text{R}} Q\left(\sqrt{2K(\theta_{\text{R}})}, \sqrt{2[K(\theta_{\text{R}}) + 1]\zeta \ell_{\text{UR}}^{\alpha(\theta_{\text{R}})}/\gamma_{\text{U}}}\right) dr_{\text{R}}, \end{aligned} \quad (76)$$

where $d\mathcal{C}$ is the surface element and (76) follows from the fact that $K(\theta_{\text{R}}) = K(\tan^{-1}(h/r_{\text{R}}))$ and $\ell_{\text{UR}} = \sqrt{h^2 + r_{\text{R}}^2}$ adopt the same value in any φ_{R} . Therefore, the probability mass function of $|\mathcal{A}|$ can be expressed as

$$\mathbb{P}(|\mathcal{A}| = i) = \frac{\mu_{\mathcal{A}}(h)^i}{i!} e^{-\mu_{\mathcal{A}}(h)}. \quad (77)$$

As a result of the PPP property, the locations of the relay nodes in \mathcal{A} , i.e. $\text{R}_1, \text{R}_2, \dots, \text{R}_i$ are identical independent (i.i.d) RVs indicated by R . Thus following the assumption that the fading powers between any pair of nodes are independent RVs, $\Gamma_{\text{R}_1\text{D}}, \Gamma_{\text{R}_2\text{D}}, \dots, \Gamma_{\text{R}_i\text{D}}$ become i.i.d RVs as well which are indicated by Γ_{RD} . Therefore, the conditional probability term in (74) can be calculated as

$$\begin{aligned} \mathbb{P}(\Gamma_{\text{R}_j\text{D}} \leq \zeta \mid |\mathcal{A}| = i) &= \mathbb{P}(\max\{\Gamma_{\text{R}_1\text{D}}, \Gamma_{\text{R}_2\text{D}}, \dots, \Gamma_{\text{R}_i\text{D}}\} \leq \zeta) \\ &= \prod_{j=1}^i \mathbb{P}(\Gamma_{\text{R}_j\text{D}} \leq \zeta) = \mathbb{P}(\Gamma_{\text{RD}} \leq \zeta)^i. \end{aligned} \quad (78)$$

By representing any specific location of R as $\text{R} : (r_{\text{R}}, \varphi_{\text{R}})$ one can write

$$\mathbb{P}(\Gamma_{\text{RD}} \leq \zeta) = \int_{\mathcal{C}} \mathbb{P}(\Gamma_{\text{RD}} \leq \zeta \mid \text{R} : (r_{\text{R}}, \varphi_{\text{R}})) \frac{\lambda_{\mathcal{A}}(r_{\text{R}}, \varphi_{\text{R}}, h)}{\mu_{\mathcal{A}}(h)} d\mathcal{C} \quad (79a)$$

$$= \frac{1}{\mu_{\mathcal{A}}(h)} \int_{\mathcal{C}} \mathbb{P}\left(\frac{AP_{\text{R}}}{N_0 \ell_{\text{RD}}^{\alpha_0}} \Omega_{\text{RD}} \leq \zeta \mid \text{R} : (r_{\text{R}}, \varphi_{\text{R}})\right) \times \lambda_{\mathcal{A}}(r_{\text{R}}, \varphi_{\text{R}}, h) d\mathcal{C} \quad (79b)$$

$$= \frac{1}{\mu_{\mathcal{A}}(h)} \int_{\mathcal{C}} \left[1 - Q\left(\sqrt{2\kappa_0}, \sqrt{2(\kappa_0 + 1)\zeta \ell_{\text{RD}}^{\alpha_0}/\gamma_{\text{R}}}\right)\right] \times \lambda_{\mathcal{A}}(r_{\text{R}}, \varphi_{\text{R}}, h) d\mathcal{C} \quad (79c)$$

$$= \frac{\lambda}{\mu_{\mathcal{A}}(h)} \int_0^{2\pi} \int_0^{r_{\text{C}}^{\text{rc}}} r_{\text{R}} \left[1 - Q\left(\sqrt{2\kappa_0}, \sqrt{2(\kappa_0 + 1)\zeta \ell_{\text{RD}}^{\alpha_0}/\gamma_{\text{R}}}\right)\right] \times Q\left(\sqrt{2K(\theta_{\text{R}})}, \sqrt{2[K(\theta_{\text{R}}) + 1]\zeta \ell_{\text{UR}}^{\alpha(\theta_{\text{R}})}/\gamma_{\text{U}}}\right) dr_{\text{R}} d\varphi_{\text{R}}. \quad (79d)$$

$$\times Q\left(\sqrt{2K(\theta_{\text{R}})}, \sqrt{2[K(\theta_{\text{R}}) + 1]\zeta \ell_{\text{UR}}^{\alpha(\theta_{\text{R}})}/\gamma_{\text{U}}}\right) dr_{\text{R}} d\varphi_{\text{R}}. \quad (79e)$$

In (79b) the expression in (3) is used, (79c) follows from the fact that Ω_{RD} has a non-central chi-square PDF with unit mean where $\gamma_{\text{R}} = AP_{\text{R}}/N_0$, and in (79e) the relation in (75c) is replaced.

Now from (74), (77) and (78) one can write

$$\begin{aligned} \mathcal{P}_{\text{out}}^{\text{rc}}(r_{\text{D}}, h) &= \sum_{i=0}^{\infty} \mathbb{P}(\Gamma_{\text{RD}} \leq \zeta)^i \frac{\mu_{\mathcal{A}}(h)^i}{i!} e^{-\mu_{\mathcal{A}}(h)} \\ &= e^{-\mu_{\mathcal{A}}(h)} \sum_{i=0}^{\infty} \frac{[\mu_{\mathcal{A}}(h) \mathbb{P}(\Gamma_{\text{RD}} \leq \zeta)]^i}{i!} \\ &= e^{-\mu_{\mathcal{A}}(h)} e^{\mu_{\mathcal{A}}(h) \mathbb{P}(\Gamma_{\text{RD}} \leq \zeta)} = e^{-\mu_{\mathcal{A}}(h) + \mu_{\mathcal{A}}(h) \mathbb{P}(\Gamma_{\text{RD}} \leq \zeta)}, \end{aligned} \quad (80)$$

where (80) is obtained using the Taylor series expansion of exponential function. From (76), (79e) and (80) we obtain the desired result.

APPENDIX E
PATH LOSS EXPONENT $\alpha(\theta)$

Here we discuss the proposed expression for $\alpha(\theta)$ in (31) by using a model reported in [15] in which the path loss can be written as

$$\begin{aligned} \text{PL}_1(\theta, \ell) &= \text{PL}_{\text{LoS}}(\ell) \cdot \mathcal{P}_{\text{LoS}}(\theta) \\ &\quad + \text{PL}_{\text{NLoS}}(\ell) \cdot [1 - \mathcal{P}_{\text{LoS}}(\theta)], \end{aligned} \quad (81a)$$

where

$$\text{PL}_{\text{LoS}}(\ell) = 20 \log\left(\frac{4\pi f}{c} \ell\right) + \sigma_{\text{LoS}}, \quad (81b)$$

$$\text{PL}_{\text{NLoS}}(\ell) = 20 \log\left(\frac{4\pi f}{c} \ell\right) + \sigma_{\text{NLoS}}, \quad (81c)$$

$\mathcal{P}_{\text{LoS}}(\theta)$ is given in (32), f is the system frequency, c is the speed of light, ℓ is the distance between transmitter and receiver, and σ_{LoS} and σ_{NLoS} are excessive path loss corresponded to the LoS and NLoS signals respectively which

are constants being independent of θ . On the other hand, in our model presented in Section II the path loss in dB is

$$PL_2(\theta, \ell) = 10\alpha(\theta) \log(\ell) + A_{dB}, \quad (82)$$

where $A_{dB} = 10 \log(A)$. Thus in order to fit the two models one can write

$$\alpha(\theta) = \frac{PL_1(\theta, \ell) - A_{dB}}{10 \log(\ell)}. \quad (83)$$

However the above equation results in a distance-dependent $\alpha(\theta)$. To resolve this issue we take the average of $\alpha(\theta)$ obtained from (83) over a reasonable range of communication, $\ell_1, \ell_2, \dots, \ell_N$, for a UAV. Therefore, one obtains

$$\alpha(\theta) = \frac{1}{N} \sum_{i=1}^N \frac{PL_1(\theta, \ell_i) - A_{dB}}{10 \log(\ell_i)}, \quad (84)$$

which can be rewritten as

$$\alpha(\theta) = a_1 \cdot \mathcal{P}_{LoS}(\theta) + a_2, \quad (85)$$

where a_1 and a_2 are determined by the type of environment (suburban, urban, dense urban, . . .) and system frequency, and given by

$$a_1 = \sum_{i=1}^N \frac{PL_{LoS}(\ell_i) - PL_{NLoS}(\ell_i)}{10N \log(\ell_i)},$$

$$a_2 = \sum_{i=1}^N \frac{PL_{NLoS}(\ell_i) - A_{dB}}{10N \log(\ell_i)}. \quad (86)$$

It is to be noted that $PL_1(\theta, \ell)$ limits the model for large θ s where free space assumption is met. To clarify this fact, assume that θ_0 is a very low angle where $\mathcal{P}_{LoS}(\theta_0) \rightarrow 0$. Thus, using (81) one obtains

$$PL_1(\theta_0, \ell) \cong PL_{NLoS}(\ell) = 20 \log \left(\frac{4\pi f}{c} \ell \right) + \sigma_{NLoS}, \quad (87)$$

where σ_{NLoS} is a constant parameter independent from distance ℓ . Therefore, the above equation is not following the well-known path loss behavior of the G2G communication where the path loss exponent is expected to be larger than 3. However, our proposed model is capable of resolving this issue by setting an appropriate value for α_0 in a way that satisfies the G2G communication propagation characteristics for low angles.

REFERENCES

- [1] "Connecting the world from the sky," Facebook, Cambridge, MA, USA, Tech. Rep., 2014.
- [2] S. Katikala, "Google project loon," *Sight, Rivier Acad. J.*, vol. 10, no. 2, 2014.
- [3] (2015). *Amazon Prime Air*. [Online]. Available: <http://www.amazon.com/b?node=8037720011>
- [4] *Absolute (Aerial Base Stations With Opportunistic Links for Unexpected and Temporary Events)*. [Online]. Available: <http://www.absolute-project.eu>
- [5] S.-Y. Lien, K.-C. Chen, and Y. Lin, "Toward ubiquitous massive accesses in 3GPP machine-to-machine communications," *IEEE Commun. Mag.*, vol. 49, no. 4, pp. 66–74, Apr. 2011.
- [6] H. S. Dhillon, H. Huang, and H. Viswanathan. (Apr. 2015). "Wide-area wireless communication challenges for the Internet of Things." [Online]. Available: <https://arxiv.org/abs/1504.03242>
- [7] M. Mozaffari, W. Saad, M. Bennis, and M. Debbah. (Mar. 2017). "Mobile unmanned aerial vehicles (UAVs) for energy-efficient Internet of Things communications." [Online]. Available: <https://arxiv.org/abs/1703.05401>
- [8] Y. Zeng and R. Zhang, "Energy-efficient UAV communication with trajectory optimization," *IEEE Trans. Wireless Commun.*, vol. 16, no. 6, pp. 3747–3760, Jun. 2017.
- [9] S. Rohde and C. Wietfeld, "Interference aware positioning of aerial relays for cell overload and outage compensation," in *Proc. IEEE Veh. Technol. Conf. (VTC Fall)*, Sep. 2012, pp. 1–5.
- [10] A. Merwady and I. Guvenc, "Uav assisted heterogeneous networks for public safety communications," in *Proc. IEEE Wireless Commun. Netw. Conf. Workshops (WCNCW)*, Mar. 2015, pp. 329–334.
- [11] M. M. Azari, F. Rosas, and S. Pollin, "Drone deployment in cellular networks: Coexistence and trade-offs analysis," *IEEE J. Sel. Areas Commun.*, to be published.
- [12] Y. Zeng, R. Zhang, and T. J. Lim, "Wireless communications with unmanned aerial vehicles: Opportunities and challenges," *IEEE Commun. Mag.*, vol. 54, no. 5, pp. 36–42, May 2016.
- [13] X. Li, D. Guo, H. Yin, and G. Wei, "Drone-assisted public safety wireless broadband network," in *Proc. IEEE Wireless Commun. Netw. Conf. Workshops (WCNCW)*, Mar. 2015, pp. 323–328.
- [14] Y. Zeng, R. Zhang, and T. J. Lim, "Throughput maximization for UAV-enabled mobile relaying systems," *IEEE Trans. Commun.*, vol. 64, no. 12, pp. 4983–4996, Dec. 2016.
- [15] A. Al-Hourani, S. Kandeepan, and S. Lardner, "Optimal LAP altitude for maximum coverage," *IEEE Wireless Commun. Lett.*, vol. 3, no. 6, pp. 569–572, Dec. 2014.
- [16] R. I. Bor-Yaliniz, A. El-Keyi, and H. Yanikomeroglu, "Efficient 3-D placement of an aerial base station in next generation cellular networks," in *Proc. IEEE Int. Conf. Commun. (ICC)*, May 2016, pp. 1–5.
- [17] M. Mozaffari, W. Saad, M. Bennis, and M. Debbah, "Efficient deployment of multiple unmanned aerial vehicles for optimal wireless coverage," *IEEE Commun. Lett.*, vol. 20, no. 8, pp. 1647–1650, Aug. 2016.
- [18] D. W. Matolak, "Air-ground channels & models: Comprehensive review and considerations for unmanned aircraft systems," in *Proc. IEEE Aersp. Conf.*, Mar. 2012, pp. 1–17.
- [19] J. N. Laneman, D. N. C. Tse, and G. W. Wornell, "Cooperative diversity in wireless networks: Efficient protocols and outage behavior," *IEEE Trans. Inf. Theory*, vol. 50, no. 12, pp. 3062–3080, Dec. 2004.
- [20] H. Wang, S. Ma, T.-S. Ng, and H. V. Poor, "A general analytical approach for opportunistic cooperative systems with spatially random relays," *IEEE Trans. Wireless Commun.*, vol. 10, no. 12, pp. 4122–4129, Dec. 2011.
- [21] H. Yu, I.-H. Lee, and G. L. Stüber, "Outage probability of decode-and-forward cooperative relaying systems with co-channel interference," *IEEE Trans. Wireless Commun.*, vol. 11, no. 1, pp. 266–274, Jan. 2012.
- [22] A. Behnad, A. M. Rabiei, N. C. Beaulieu, and H. Hajizadeh, "Generalized analysis of dual-hop DF opportunistic relaying with randomly distributed relays," *IEEE Commun. Lett.*, vol. 17, no. 6, pp. 1057–1060, Jun. 2013.
- [23] M. M. Eddaghel, U. N. Mannai, G. J. Chen, and J. A. Chambers, "Outage probability analysis of an amplify-and-forward cooperative communication system with multi-path channels and max-min relay selection," *IET Commun.*, vol. 7, no. 5, pp. 408–416, Mar. 2013.
- [24] M. M. Azari, A. M. Rabiei, and A. Behnad, "Probabilistic relay assignment strategy for cooperation networks with random relays," *IET Commun.*, vol. 8, no. 6, pp. 930–937, Apr. 2014.
- [25] M. M. Azari, F. Rosas, K.-C. Chen, and S. Pollin, "Optimal UAV positioning for terrestrial-aerial communication in presence of fading," in *Proc. IEEE Global Commun. Conf. (GLOBECOM)*, Dec. 2016, pp. 1–7.
- [26] M. M. Azari, F. Rosas, A. Chiumento, K.-C. Chen, and S. Pollin, "Coverage and power gain of aerial versus terrestrial base stations," in *Advances in Ubiquitous Networking*. Singapore: Springer, 2017, pp. 627–636.
- [27] M. M. Azari, F. Rosas, K.-C. Chen, and S. Pollin, "Joint sum-rate and power gain analysis of an aerial base station," in *Proc. IEEE Globecom Workshops (GC Wkshps)*, Dec. 2016, pp. 1–6.
- [28] B. Van Der Bergh, A. Chiumento, and S. Pollin, "LTE in the sky: Trading off propagation benefits with interference costs for aerial nodes," *IEEE Commun. Mag.*, vol. 54, no. 5, pp. 44–50, May 2016.
- [29] S. Kandeepan, K. Gomez, L. Reynaud, and T. Rasheed, "Aerial-terrestrial communications: Terrestrial cooperation and energy-efficient transmissions to aerial base stations," *IEEE Trans. Aersp. Electron. Syst.*, vol. 50, no. 4, pp. 2715–2735, Oct. 2014.

- [30] S. Kandeepan, K. Gomez, T. Rasheed, and L. Reynaud, "Energy efficient cooperative strategies in hybrid aerial-terrestrial networks for emergencies," in *Proc. IEEE 22nd Int. Symp. Pers. Indoor Mobile Radio Commun. (PIMRC)*, Sep. 2011, pp. 294–299.
- [31] M. K. Simon and M.-S. Alouini, *Digital Communication Over Fading Channels*, vol. 95. Hoboken, NJ, USA: Wiley, 2005.
- [32] J. Hagenauer, F. Dolainsky, E. Lutz, W. Papke, and R. Schweikert, "The maritime satellite communication channel–channel model, performance of modulation and coding," *IEEE J. Sel. Areas Commun.*, vol. 5, no. 4, pp. 701–713, May 1987.
- [33] S. Shimamoto *et al.*, "The channel characterization and performance evaluation of mobile communication employing stratospheric platform," *IEICE Trans. Commun.*, vol. 89, no. 3, pp. 937–944, 2006.
- [34] R. T. Short, "Computation of Rice and noncentral chi-squared probabilities," *PhaseLocked Syst.*, Ottawa, ON, Canada, Tech. Rep. PHS0254, 2012.
- [35] J. Segura, "Bounds for ratios of modified Bessel functions and associated turán-type inequalities," *J. Math. Anal. Appl.*, vol. 374, no. 2, pp. 516–528, 2011.
- [36] S. M. Prokis and G. John, *Digital Communications*. New York, NY, USA: McGraw-Hill, 2008.
- [37] J. F. C. Kingman, *Poisson Processes*. Oxford, U.K.: Oxford Science, 1993.



Mohammad Mahdi Azari received the B.Sc. and M.Sc. degrees in electrical and communication engineering from the University of Tehran, Tehran, Iran. He is currently pursuing the Ph.D. degree with the Department of Electrical Engineering, KU Leuven, Belgium. His main research interests include unmanned aerial vehicle communication and networking, modeling and analysis of cellular networks, and mmWave communication. He has received the Iran's National Elites Foundation Award.



Fernando Rosas received the B.A. degree in music composition and philosophy, the B.Sc. degree in mathematics, and the M.S. and Ph.D. degrees in engineering sciences from the Pontificia Universidad Católica de Chile (PUC). He is currently a Research Fellow with the Centre of Complexity Science, Department of Mathematics, Imperial College London. His research interests lay in the interface between communication theory, complexity science, and neuroscience. He received the Academic Award from the Department of Mathematics, PUC, having

the best scores of his promotion, and he was a recipient of a CONICYT Doctoral Fellowship from the Chilean Ministry of Education in 2008, a "F+" Scholarship from KU Leuven University in 2013, and a Marie Slodowska-Curie Individual Fellowship from the European Union in 2016.



Kwang-Cheng Chen (M'89–SM'94–F'07) received the B.S. degree from National Taiwan University in 1983, and the M.S. and Ph.D. degrees from the University of Maryland at College Park, College Park, USA, in 1987 and 1989, respectively, all in electrical engineering. From 1987 to 1998, he was with SSE, COMSAT, IBM Thomas J. Watson Research Center, and National Tsing Hua University, involved in the mobile communications and networks. From 1998 to 2016, he was a Distinguished Professor with National Taiwan University, Taipei, Taiwan, and also served as the Director of the Graduate Institute of Communication Engineering and the Communication Research Center, and the Associate Dean for Academic Affairs, College of Electrical Engineering and Computer Science from 2009 to 2015. Since 2016, he has been with the Department of Electrical Engineering, University of South Florida, Tampa, FL, USA. His recent research interests include wireless networks, cybersecurity, cyber-physical systems, social networks, and data analytics. He has received a number of awards, including the 2011 IEEE COMSOC WTC Recognition Award, the 2014 IEEE Jack Neubauer Memorial Award, and the 2014 IEEE COMSOC AP Outstanding Paper Award. He has been actively involved in the organization of various IEEE conferences as the General/TPC Chair/Co-Chair, and has served in editorships with a few IEEE journals. He also actively participates in and has contributed essential technology to various IEEE 802, Bluetooth, and LTE and LTE-A wireless standards.



Sofie Pollin received the Ph.D. degree (Hons.) from KU Leuven in 2006. From 2006 to 2008, she continued her research on wireless communication, energy-efficient networks, cross-layer design, coexistence, and cognitive radio at UC Berkeley. In 2008, she returned to imec to become a Principal Scientist in the Green Radio Team. Since 2012, she has been a Tenure Track Assistant Professor with the Electrical Engineering Department, KU Leuven. Her research centers around networked systems that require networks that are ever more dense, heterogeneous, battery powered, and spectrum constrained. She is a BAEF and Marie Curie Fellow.